

OPTIMAL EXPERIMENTAL DESIGN FOR INVERSE PROBLEMS IN THE PRESENCE OF OBSERVATION CORRELATIONS*

AHMED ATTIA[†] AND EMIL CONSTANTINESCU^{†‡}

Abstract. Optimal experimental design (OED) is the general formalism of sensor placement and decisions about the data collection strategy for engineered or natural experiments. This approach is prevalent in many critical fields such as battery design, numerical weather prediction, geosciences, and environmental and urban studies. State-of-the-art computational methods for experimental design, however, do not accommodate correlation structure in observational errors produced by many expensive-to-operate devices such as X-ray machines or radar and satellite retrievals. Discarding evident data correlations leads to biased results, poor data collection decisions, and waste of valuable resources. We present a general formulation of the OED formalism for model-constrained large-scale Bayesian linear inverse problems, where measurement errors are generally correlated. The proposed approach utilizes the Hadamard product of matrices to formulate the weighted likelihood and is valid for both finite- and infinite-dimensional Bayesian inverse problems. Extensive numerical experiments are carried out for empirical verification of the proposed approach by using an advection-diffusion model, where the objective is to optimally place a small set of sensors, under a limited budget, to predict the concentration of a contaminant in a closed and bounded domain.

Key words. Optimal experimental design (OED), Inverse problems, Correlated observations, Data assimilation

AMS subject classifications. 62K05, 35Q62, 62F15, 35R30, 35Q93, 65C60

1. Introduction. Sensor placement is the problem of determining the optimal positions of a given number of sensors from a set of candidate locations. This problem is widely formulated as an optimal experimental design (OED) problem [38, 20, 35, 43], where the design determines whether to activate a sensor or not. Bayesian OED for data acquisition and sensor placement has been addressed in the context of ill-posed linear inverse problems [22, 24] and nonlinear inverse problems [23, 28] and has also been considered in infinite-dimensional settings [13, 3, 6, 5, 4, 1]. In our work and the works cited above, linearity is associated with the parameter-to-observable map, which describes the relation between the quantity of interest (QoI) and the observational data.

Scalable data assimilation and uncertainty quantification methodologies have gained significant interest, especially when applied to large- to extreme-scale models, such as the atmosphere and power grid simulations [12, 18, 34, 10, 9]. The underlying principle of these methods is that information collected from observational systems is fused into computational models to produce accurate forecasts of a QoI. This QoI could, for example, refer to the model parameters, initial condition, or the model state. In Bayesian inversion, the goal is to infer the value of the QoI, through the posterior distribution of that QoI modeled as a random variable, conditioned by the noisy observational data. The quality of such assimilation systems depends heavily on the extent to which the mathematical assumptions reflect reality, as well as on the quality of the collected measurements, which in turn depends on the data acquisition schedule and the sensor placement

*Submitted to the editors August 6, 2021.

Funding: This work was partially supported by the U.S. Department of Energy, Office of Science, Advanced Scientific Computing Research Program under contract DE-AC02-06CH11357 and Laboratory Directed Research and Development (LDRD) funding from Argonne National Laboratory.

[†]Mathematics and Computer Science Division, Argonne National Laboratory, Lemont, IL (attia@mcs.anl.gov and emconsta@mcs.anl.gov).

[‡]The University of Chicago, IL.

strategy.

An optimal design improves the quality of the observational grid and the collected data and hence improves the model-based forecast made by an assimilation system. Moreover, deploying and operating observational instruments can be expensive, thus mandating the development of optimal sensor placement strategies and optimal data acquisition schedules. An optimal design is generally found by solving an optimization problem with the objective of minimizing the uncertainty of the posterior QoI under the constraints forced by the computational model. The objective function of such an optimization problem is formulated based on the choice of the optimality criterion, which is a scalar summary of the uncertainty of the Bayesian inversion QoI. For example, an A-optimal design minimizes the average variance, and a D-optimal design minimizes the generalized variance, which is equivalent to maximizing the differential Shannon information content of the inversion QoI [38].

The presence of observation spatiotemporal error correlations in OED for inverse problems poses a significant challenge [44]. A common approach, which is followed for simplicity in solving model-constrained OED problems, is to drop spatiotemporal correlations and assume that observation errors are temporally and spatially uncorrelated. This approach, however, can be restrictive and is even violated in many applications where a single instrument is used to collect measurements at various orientations, such as X-ray machines, satellites, and light detection and ranging radars.

The statistics literature provides a wealth of treatments of correlated observations in several OED scenarios and settings [17, 32, 33, 37, 16]. For example, the ordinary least-squares approach for inversion and the D-optimality criterion is adopted in [44] to avoid inaccuracies or lack of knowledge of the observation correlation structure. Additionally, OED for correlated observations has been considered in the context of linear regression models, for example in [19, 45]. Nevertheless, in the context of Bayesian inverse problems, more work is needed to provide simple algorithmic OEDs that are suitable for multiple choices of the optimality criterion and are capable of properly handling correlations in observational errors.

In this work we present a generalized OED formulation based on the Hadamard product of the observation precision matrix with a symmetric weighting kernel, where the observation errors are generally correlated. In this case, the covariances of the observation errors, manifested in the weighted data likelihood, could form a diagonal, a block diagonal, or even a full space-time covariance matrix. This approach provides a generalized formulation of the OED optimality criteria and the associated gradients, where it takes into account the correlation structure of observational errors. Moreover, it enables controlling the influence of observational correlations on the experimental design, for example, by ignoring the effect of spurious correlations, using a space-time weighting kernel. We show that the traditional OED formulation is a special case of the proposed formulation, where the weighting kernel takes a specific form. In fact, the new formulation adds a layer of flexibility to the standard formulation of OED in the context of Bayesian inversion and is suitable for both finite- and infinite-dimensional Bayesian linear inversion frameworks. Moreover, the presented approach converts the OED constrained optimization problem into an unconstrained optimization problem, which enables utilizing a plethora of efficient numerical optimization routines.

The rest of the paper is structured as follows. Section 2 provides the mathematical background and describes the standard formulation of optimal design of experiments for Bayesian linear inverse problems. The proposed approach for handling errors in observation correlations is described in Section 3, with detailed derivation of formulae given in the appendices included in the supplement.

tary material. The setup and results of numerical experiments are given in [Section 4](#). Concluding remarks are presented in [Section 5](#).

2. Background. Here we review the elements of Bayesian inversion and OED for Bayesian inverse problems governed by computational models, such as partial differential equations (PDEs).

2.1. Bayesian inverse problem. A forward problem describes the relationship between model parameters and observational data. The vast majority of large-scale simulation models follow the forward model described by $\mathbf{y} = \mathcal{F}(\theta) + \delta$, where $\theta \in \mathbb{R}^{N_{\text{state}}}$ is the model parameter and $\mathbf{y} \in \mathbb{R}^{N_{\text{obs}}}$ is the observational data. The forward map \mathcal{F} is a discretized parameter-to-observable operator that maps a model parameter into the observation space, and $\delta \in \mathbb{R}^{N_{\text{obs}}}$ accounts for measurement noise. We restrict the discussion in this work to the case of linear models, that is, $\mathcal{F}(\theta) = \mathbf{F}\theta$:

$$(2.1) \quad \mathbf{y} = \mathbf{F}\theta + \delta.$$

The parameter θ is generally modeled as a random variable with a Gaussian prior $\mathcal{N}(\theta_{\text{pr}}, \mathbf{\Gamma}_{\text{pr}})$. In the Gaussian framework, the observational noise is assumed to be Gaussian, that is, $\delta \sim \mathcal{N}(\mathbf{0}, \mathbf{\Gamma}_{\text{noise}})$, where $\mathbf{\Gamma}_{\text{noise}}$ is the observation error covariance matrix. In this case, the data likelihood is

$$(2.2) \quad \mathcal{L}(\mathbf{y}|\theta) \propto \exp\left(-\frac{1}{2} \|\mathbf{F}\theta - \mathbf{y}\|_{\mathbf{\Gamma}_{\text{noise}}^{-1}}^2\right),$$

where the weighted norm is defined as $\|\mathbf{x}\|_{\mathbf{A}}^2 = \mathbf{x}^T \mathbf{A} \mathbf{x}$.

The inverse problem involves retrieving the underlying model parameter θ from noisy measurements \mathbf{y} , given the specification of prior and observation noise uncertainties. Specifically, in Bayesian inversion we seek the posterior distribution of θ conditioned by observational data \mathbf{y} . For a linear forward operator \mathbf{F} , the posterior is Gaussian $\mathcal{N}(\theta_{\text{post}}^{\mathbf{y}}, \mathbf{\Gamma}_{\text{post}})$ with

$$(2.3) \quad \theta_{\text{post}}^{\mathbf{y}} = \mathbf{\Gamma}_{\text{post}} (\mathbf{\Gamma}_{\text{pr}}^{-1} \theta_{\text{pr}} + \mathbf{F}^* \mathbf{\Gamma}_{\text{noise}}^{-1} \mathbf{y}), \quad \mathbf{\Gamma}_{\text{post}} = (\mathbf{F}^* \mathbf{\Gamma}_{\text{noise}}^{-1} \mathbf{F} + \mathbf{\Gamma}_{\text{pr}}^{-1})^{-1} = \mathbf{H}^{-1},$$

where \mathbf{F}^* is the adjoint of the forward operator \mathbf{F} . Here the posterior mean $\theta_{\text{post}}^{\mathbf{y}}$ provides a posterior estimate of the true value of the parameter θ_{true} , given the prior mean θ_{pr} , the data \mathbf{y} , and the associated uncertainties.

We note that the Hessian \mathbf{H} of the negative log of the posterior probability density function (PDF) is equal to the posterior precision matrix $\mathbf{\Gamma}_{\text{post}}^{-1}$ and is independent from the data. Thus, in the linear Gaussian case one can completely describe the posterior covariances, given the forward operator and both prior and observation noise covariances. Unlike the linear case, however, if the forward operator \mathcal{F} is nonlinear, the posterior covariance depends on the observational data, and the OED problem becomes more difficult and is beyond the scope of this work.

2.2. Goal-oriented Bayesian inverse problem. Solving an inverse problem is often an intermediate step, where the inversion parameter, such as the inferred model parameter, is then used to make further prediction of a goal QoI. We consider the QoI of the form $\gamma = \mathbf{P}\theta \in \mathbb{R}^{N_{\text{goal}}}$, where \mathbf{P} is a linear *goal operator* [7]. A simple example of \mathbf{P} is an integral operator that evaluates the expected value of the inferred parameter. We follow this general formulation hereafter since the standard Bayesian inverse problem is a special case, where \mathbf{P} is set to the identity operator

\mathcal{I} . Given the distribution of the model parameter, the prior of γ is Gaussian $\mathcal{N}(\gamma_{\text{pr}}, \Sigma_{\text{pr}})$, with $\gamma_{\text{pr}} = \mathbf{P}\theta_{\text{pr}}$, and $\Sigma_{\text{pr}} = \mathbf{P}\Gamma_{\text{pr}}\mathbf{P}^*$. The posterior of γ is also Gaussian $\mathcal{N}(\gamma_{\text{post}}, \Sigma_{\text{post}})$, with

$$(2.4) \quad \gamma_{\text{post}} = \mathbf{P}\Gamma_{\text{post}} \left(\Gamma_{\text{pr}}^{-1}\theta_{\text{pr}} + \mathbf{F}^*\Gamma_{\text{noise}}^{-1}\mathbf{y} \right), \quad \Sigma_{\text{post}} = \mathbf{P} \left(\mathbf{F}^*\Gamma_{\text{noise}}^{-1}\mathbf{F} + \Gamma_{\text{pr}}^{-1} \right)^{-1} \mathbf{P}^*.$$

The exact form of the adjoint of the forward operator \mathbf{F}^* and the adjoint of the goal operator \mathbf{P}^* depend on the problem at hand. Specific instances will be discussed in [Section 4](#) in the context of numerical experiments.

2.3. Bayesian OED. In Bayesian OED, we seek a design for the data acquisition process. The specific definition of an experimental design, in general, is problem dependent. For example, an experimental design $\zeta \in \Xi$ can be associated with the configuration of an observational grid; that is, the experimental design describes the sensor placement strategy. In this case, an experimental design is said to be optimal if it minimizes the posterior uncertainty of the solution of an inverse problem in some sense. The optimal design ζ^{opt} in the context of an inverse problem is defined by an *optimality criterion*, which in general is a scalar functional $\Psi(\cdot)$ that depends on the posterior uncertainty of the inversion QoI. In the linear Gaussian settings, the optimality criterion is generally set as a scalar summary of the posterior covariance matrix. The traditional alphabetic criteria including A- and D-optimality are the most popular choices [\[2\]](#). An A-optimal design $\zeta^{\text{A-opt}}$ minimizes the trace of the posterior covariance, while the D-optimal design $\zeta^{\text{D-opt}}$ minimizes its determinant (or equivalently the log-determinant):

$$(2.5) \quad \zeta^{\text{A-opt}} = \arg \min_{\zeta \in \Xi} \Psi^{\text{GA}}(\zeta) := \text{Tr}(\Sigma_{\text{post}}(\zeta)); \quad \zeta^{\text{D-opt}} = \arg \min_{\zeta \in \Xi} \Psi^{\text{GD}}(\zeta) := \log \det(\Sigma_{\text{post}}(\zeta)).$$

These optimality criteria are typically augmented by regularization and sparsification terms that are discussed in later sections.

2.4. Bayesian OED for sensor placement. In the sensor placement problems, we seek the *optimal* subset of sensors of size λ , from n_s candidate locations. In this case, the design ζ is a vector of binary entries, whose components can be interpreted as sensors being *active* or *inactive*; that is, $\zeta \in \Xi := \{0, 1\}^{n_s}$. Solving a binary OED problem for sensor placement is computationally infeasible for large-scale problems. In practice, the design weights, that is, the integrality of entries $\zeta_i; i = 1, 2, \dots, n_s$, are *relaxed* to take values in the interval $[0, 1]$; that is, $\zeta \in \Xi := [0, 1]^{n_s}$. Then a sparsification is enforced by adding a suitable regularization term to the optimality objective [\(2.5\)](#).

The design enters the inverse problem formulation through the data likelihood as a set of observation weights. Specifically, the observation covariance Γ_{noise} is replaced with a weighted version $\mathbf{W}_{\Gamma}(\zeta)$, resulting in the weighted data likelihood

$$(2.6) \quad \mathcal{L}(\mathbf{y}|\theta; \zeta) \propto \exp \left(-\frac{1}{2} \|\mathbf{F}\theta - \mathbf{y}\|_{\mathbf{W}_{\Gamma}(\zeta)}^2 \right).$$

The weighted posterior covariance of the inferred QoI in this case is

$$(2.7) \quad \Sigma_{\text{post}}(\zeta) = \mathbf{P} (\mathbf{H}(\zeta))^{-1} \mathbf{P}^* = \mathbf{P} (\mathbf{F}^* \mathbf{W}_{\Gamma}(\zeta) \mathbf{F} + \Gamma_{\text{pr}}^{-1})^{-1} \mathbf{P}^*.$$

A common approach to define the weighted inverse covariance matrix $\mathbf{W}_{\Gamma}(\zeta)$ is to introduce a weighting matrix $\mathbf{W}(\zeta)$ and use the form $\mathbf{W}_{\Gamma}(\zeta) := \mathbf{W}^{\frac{1}{2}}(\zeta) \Gamma_{\text{noise}}^{-1} \mathbf{W}^{\frac{1}{2}}(\zeta)$. The design matrix $\mathbf{W} \in$

$\mathbb{R}^{N_{\text{obs}} \times N_{\text{obs}}}$ is a symmetric weighting matrix parameterized by the design ζ . In sensor placement problems, the design is a vector containing weights assigned to each candidate sensor location $\zeta = (\zeta_1, \zeta_2, \dots, \zeta_{n_s})^T$, and the weighting matrix is a diagonal matrix with design weights on the diagonal; that is, $\mathbf{W} = \text{diag}(\zeta)$. An alternative approach is to use the form $\mathbf{W}_\Gamma := \mathbf{\Gamma}_{\text{noise}}^{-\frac{1}{2}} \mathbf{W} \mathbf{\Gamma}_{\text{noise}}^{-\frac{1}{2}}$. Little attention is given in the literature to the difference between these two forms, mainly because in many applications the observations are assumed to be uncorrelated, resulting in a diagonal covariance matrix $\mathbf{\Gamma}_{\text{noise}}$. In this case these two forms are equivalent. In general, however, they are not. The latter form simplifies the derivation of the gradient of optimality criterion with respect to the design; however, the interpretability of its effect is not intuitive. On the other hand, the former form weighs the sensor observations, based on their contributed information gain, resulting in a reduction in the QoI posterior uncertainty.

In time-dependent settings, the dynamical model is simulated over a window containing observation time instances t_1, t_2, \dots, t_{n_t} . Assuming the design weights associated with candidate observational gridpoints are fixed over time, the weighting matrix $\mathbf{W} \in \mathbb{R}^{N_{\text{obs}} \times N_{\text{obs}}}$ can be defined as $\mathbf{W} = \mathbf{I}_{n_t} \otimes \text{diag}(\zeta)$ with $\mathbf{I}_{n_t} \in \mathbb{R}^{n_t \times n_t}$ an identity matrix and $N_{\text{obs}} = n_s n_t$. Here \otimes is the matrix Kronecker product. If the observational noise is temporally uncorrelated, then the covariance $\mathbf{\Gamma}_{\text{noise}}$ is generally an $N_{\text{obs}} \times N_{\text{obs}}$ block diagonal matrix $\mathbf{\Gamma}_{\text{noise}} = \bigoplus_{m=1}^{n_t} (\mathbf{R}_m)$, where \bigoplus is the matrix direct sum and $\mathbf{R}_m \in \mathbb{R}^{n_s \times n_s}$ models the spatial covariances between observation errors prescribed at time instance t_m . Note that the matrix direct sum is equivalent to the matrix Kronecker product with an identity matrix only if the entries of the direct sum are identical.

If the observation correlations are time independent, namely, $\mathbf{R}_m = \mathbf{R}, \forall m$, then $\mathbf{\Gamma}_{\text{noise}} = \mathbf{I}_{n_t} \otimes \mathbf{R}$. In the presence of spatiotemporal correlations, the covariance matrix $\mathbf{\Gamma}_{\text{noise}}$ becomes a dense symmetric block matrix with the m th block \mathbf{R}_{mn} describing covariances between observation gridpoints at time instances t_m and t_n , respectively.

The standard Bayesian OED formulation, discussed above, is ideal for spatially and temporally uncorrelated observation errors. However, it may not properly account for spatiotemporal correlations, and it is harder to apply when the design is allowed to vary over time. Specifically, the role of the relaxed design matrix is to weight covariances between candidate sensor locations—a maximum weight of 1 means activating the corresponding sensors, and a minimum weight of 0 means deactivating them—based on their contribution to the OED optimality objective. Thus, the weighting matrix \mathbf{W} needs to be applied to the observation error covariance matrix, and not to the precision matrix [30]. Moreover, the formulation does not provide enough flexibility for handling the effect of spurious observation correlations that might be introduced, for example, by misspecification of the observational error covariances. Furthermore, it does not provide any control over the values of design, besides the imposed bound constraints. For example, no inherent property enables imposing preference of specific values of the design variables such as observation cost constraints. In Section 3, we introduce a generalized formulation of the OED problem capable of handling these limitations.

2.5. The OED optimization problem. The relaxed OED problem for sensor placement is described by the following constrained optimization problem,

$$(2.8) \quad \zeta^{\text{opt}} = \arg \min_{\zeta \in [0, 1]^{n_s}} \mathcal{T}(\zeta) := \Psi(\zeta) + \alpha \Phi(\zeta),$$

where Ψ is the design criterion; $\Phi(\zeta) : [0, 1]^{n_s} \mapsto [0, \infty)$ is a penalty function that enforces regularization or sparsity on the design; and $\alpha > 0$ is a user-defined penalty parameter. The optimality criterion Ψ is set to Ψ^{GA} or Ψ^{GD} , defined by (2.5), for obtaining an A- or D-optimal design, respectively.

A gradient-based optimization approach is followed to numerically solve (2.8). A central piece of this procedure is the gradient of the optimality criterion Ψ . For $i = 1, 2, \dots, n_s$, the derivatives of A- and D-optimality criteria (2.5), respectively, are

$$(2.9a) \quad \frac{\partial \Psi^{\text{GA}}}{\partial \zeta_i} = -\text{Tr} \left(\mathbf{P} (\mathbf{H}(\zeta))^{-1} \mathbf{F}^* \frac{\partial \mathbf{W}_\Gamma(\zeta)}{\partial \zeta_i} \mathbf{F} (\mathbf{H}(\zeta))^{-1} \mathbf{P}^* \right),$$

$$(2.9b) \quad \frac{\partial \Psi^{\text{GD}}}{\partial \zeta_i} = \text{Tr} \left(\boldsymbol{\Sigma}_{\text{post}}^{-1}(\zeta) \mathbf{P} (\mathbf{H}(\zeta))^{-1} \mathbf{F}^* \frac{\partial \mathbf{W}_\Gamma(\zeta)}{\partial \zeta_i} \mathbf{F} (\mathbf{H}(\zeta))^{-1} \mathbf{P}^* \right),$$

where $\mathbf{H}(\zeta)$ is the weighted Hessian of the negative log of the posterior PDF $\mathbf{H}(\zeta) = \boldsymbol{\Gamma}_{\text{pr}}^{-1} + \mathbf{F}^* \mathbf{W}_\Gamma(\zeta) \mathbf{F}$. The gradient of the objective (2.8) is obtained by combining the gradient of the penalty term $\nabla_\zeta \Phi(\zeta)$ with the optimality criterion (2.9), that is, $\nabla_\zeta \mathcal{T}(\zeta) = \nabla_\zeta \Psi(\zeta) + \alpha \nabla_\zeta \Phi(\zeta)$, and is provided to the numerical optimization routine.

The general form of the derivative (2.9) shows that, to formulate the gradient, we need the derivative of the weighted observation noise matrix \mathbf{W}_Γ . The final form of the gradient depends on the specific form of the weighted observation covariance matrix \mathbf{W}_Γ . Most studies assume uncorrelated observations and derive the gradient accordingly for simplicity. In the next section, we provide a generalized formulation of the weighted noise matrix and the OED problem, with emphasis on the effect of the design on the observations and observation spatiotemporal correlations.

Deploying observational sensors can be expensive, and in general we seek a small number of sensors to accurately solve the inverse problem with minimum uncertainty levels. To achieve this goal, we choose the penalty Φ function to enforce sparsity on the optimal design. Sparsification can be achieved by using the ℓ_0 “norm” [4]; however, ℓ_0 is not a valid norm and is nondifferentiable, which leads to complications in the optimization procedure. An acceptable level of sparsification can be achieved by utilizing the ℓ_1 norm in the regularization term [3].

The solution of (2.8) is expected to be a sparse design; however, it is not necessarily binary. A binary design can be obtained from the solution of the relaxed optimization problem (2.8), for example, by applying thresholding [3, 7] or by applying a continuation procedure or by reweighting the regularization term [26, 29]. Another approach to ensure a binary design is to partition the domain and use the sum-up rounding procedure; see, for example, [39, 48]. The simplest approach is to truncate the relaxed optimal design. This can be done by activating sensors corresponding to nonvanishing weight (e.g., greater than a small-enough value,) resulting from solving the relaxed OED problem. Alternatively, given a specific budget λ , one can activate the sensors corresponding to the highest λ nonzero weights in the relaxed optimal design.

Following the approach in [3, 7], in the numerical experiments reported in Section 4, we promote sparsification by setting Φ to the ℓ_1 norm. Once a sparse optimal design is obtained, we choose the sensors corresponding to the highest λ optimal weights. Note that the discussion here is not limited by the choice of Φ and can be used with other sparsification methods.

3. OED for Correlated Observations. With observational noise being uncorrelated in space and in time, the mathematical analysis of the traditional formulation of the PDE-constrained

OED problem is simple; however, this places limitations on the applicability of the formulated framework. Here we address this issue by formulating the OED problem where the design choice is sensitive not only to the variances of the involved observational errors but also to the spatiotemporal correlations. Specifically, we introduce a generalization of the traditional OED framework, following a Hadamard product approach [27] for likelihood weighting. This will add another dimension of flexibility that will help us formulate a general OED framework capable of handling observation noise with spatiotemporal correlation.

3.1. A Schur product formulation of the OED problem. We formulate the weighted likelihood for OED as follows:

$$(3.1) \quad \mathcal{L}(\mathbf{y}|\theta; \zeta) \propto \exp\left(-\frac{1}{2} \|\mathbf{F}\theta - \mathbf{y}\|_{\mathbf{W}_\Gamma(\zeta)}^2\right),$$

$$(3.2) \quad \mathbf{W}_\Gamma(\zeta) := \mathbf{L}^\top \tilde{\mathbf{\Gamma}}_{\text{noise}}^{-1}(\zeta) \mathbf{L}, \quad \tilde{\mathbf{\Gamma}}_{\text{noise}}(\zeta) := \mathbf{L} \left(\mathbf{\Gamma}_{\text{noise}} \odot \mathbf{W}(\zeta) \right) \mathbf{L}^\top,$$

where \mathbf{L} is a sparse matrix that extracts nonzero rows/columns from the design matrix \mathbf{W}_Γ . Specifically, \mathbf{L} is a binary matrix with only one entry equal to 1 on each row, and the number of rows is equal to the number of active sensors. This formulation avoids difficulties related to the weighted covariance matrix being singular when any of the design weights is equal to zero. Here \odot is the Hadamard (Schur) product, and the matrix $\mathbf{W}(\zeta)$ is assumed to be a symmetric and doubly nonnegative—real positive semidefinite square matrix—weighting kernel whose entries are evaluated by using a weighting function

$$(3.3) \quad \varpi(t_k, t_l; \zeta_i, \zeta_j); \quad k, l = 1, 2, \dots, n_t; \quad i, j = 1, 2, \dots, n_s,$$

chosen to be symmetric, so that the weighting kernel $\mathbf{W}(\zeta)$ itself is symmetric. The symmetry here is defined over any permutation of the time indexes or the design variables. In other words, we require $\varpi(t_k, t_l; \zeta_i, \zeta_j) = \varpi(t_l, t_k; \zeta_i, \zeta_j) = \varpi(t_k, t_l; \zeta_j, \zeta_i) = \varpi(t_l, t_k; \zeta_j, \zeta_i)$.

An elementary component of the solution process of an OED problem is the gradient of the optimality criterion, namely, the partial derivatives with respect to the design variables. The exact form of the objective criterion and of the associated gradient depends mainly on the weighting kernel used to construct the weighting matrix $\mathbf{W}(\zeta)$. The derivative of the optimality criterion depends on the derivatives of the weighted observation covariance matrix (see (2.9)), that is,

$$(3.4) \quad \begin{aligned} \frac{\partial \mathbf{W}_\Gamma(\zeta)}{\partial \zeta_i} &= \frac{\partial \left(\mathbf{L}^\top \tilde{\mathbf{\Gamma}}_{\text{noise}}^{-1}(\zeta) \mathbf{L} \right)}{\partial \zeta_i} = -\mathbf{L}^\top \tilde{\mathbf{\Gamma}}_{\text{noise}}^{-1}(\zeta) \mathbf{L} \left(\mathbf{\Gamma}_{\text{noise}} \odot \frac{\partial \mathbf{W}(\zeta)}{\partial \zeta_i} \right) \mathbf{L}^\top \tilde{\mathbf{\Gamma}}_{\text{noise}}^{-1}(\zeta) \mathbf{L} \\ &= -\mathbf{W}_\Gamma(\zeta) \left(\mathbf{\Gamma}_{\text{noise}} \odot \frac{\partial \mathbf{W}(\zeta)}{\partial \zeta_i} \right) \mathbf{W}_\Gamma(\zeta), \end{aligned}$$

which requires evaluating the partial derivatives of the weighting kernel $\mathbf{W}(\zeta)$. Note that the structure of the matrix \mathbf{L} depends indirectly on the design variable; however, the entries of \mathbf{L} are constant, and thus \mathbf{L} is viewed as a constant matrix in (3.4) given any instance of the design variable ζ . In the discussion below, we consider time-dependent settings, where the states are checkpointed at the observation times for efficient evaluation and storage of the model state and the adjoints. As explained in Subsection 4.1, checkpointing is crucial for solving large-scale time-dependent Bayesian inverse problems. The case of time-independent models can be viewed as a special case of the temporally uncorrelated setup with one observation time instance.

We note that the entries of the observation error covariance matrix $\mathbf{\Gamma}_{\text{noise}}$ describe covariances between all candidate sensor locations, at all observation time instances, as discussed in [Subsection 2.4](#). The general form of the weighting function given by (3.3) enables scaling the entries of the covariance matrix $\mathbf{\Gamma}_{\text{noise}}$, where the respective weights are calculated based on both time and space. We explain this thought using a simplified example. Consider a time-dependent simulation with an observational grid with $n_s = 2$ candidate sensor locations. Assume the observations are to be collected at two time instances t_1, t_2 , respectively, with the observation error covariance matrix

$$\mathbf{\Gamma}_{\text{noise}} = \begin{bmatrix} \mathbf{R}_{1,1} & \mathbf{R}_{1,2} \\ \mathbf{R}_{2,1} & \mathbf{R}_{2,2} \end{bmatrix},$$

where each block $\mathbf{R}_{n,m} \in \mathbb{R}^{2 \times 2}$ describes the error covariances between observational gridpoints at time instances t_n, t_m , respectively, where $n, m = 1, 2$. The design $\zeta \in \Xi \subseteq \mathbb{R}^2$ is associated with the candidate sensor locations and thus is defined as $\zeta = (\zeta_1, \zeta_2)^\top$. The weighting matrix is defined as follows:

$$\mathbf{W}(\zeta) := \begin{bmatrix} \varpi(t_1, t_1; \zeta_1, \zeta_1) & \varpi(t_1, t_1; \zeta_1, \zeta_2) & \varpi(t_1, t_2; \zeta_1, \zeta_1) & \varpi(t_1, t_2; \zeta_1, \zeta_2) \\ \varpi(t_1, t_1; \zeta_2, \zeta_1) & \varpi(t_1, t_1; \zeta_2, \zeta_2) & \varpi(t_1, t_2; \zeta_2, \zeta_1) & \varpi(t_1, t_2; \zeta_2, \zeta_2) \\ \varpi(t_2, t_1; \zeta_1, \zeta_1) & \varpi(t_2, t_1; \zeta_1, \zeta_2) & \varpi(t_2, t_2; \zeta_1, \zeta_1) & \varpi(t_2, t_2; \zeta_1, \zeta_2) \\ \varpi(t_2, t_1; \zeta_2, \zeta_1) & \varpi(t_2, t_1; \zeta_2, \zeta_2) & \varpi(t_2, t_2; \zeta_2, \zeta_1) & \varpi(t_2, t_2; \zeta_2, \zeta_2) \end{bmatrix}.$$

This shows that the dimension of the design is independent from the size of the temporal domain and is generally much less than the dimension of the space-time domain.

This formulation gives more flexibility in forming the design matrix, which acts as a weighting kernel in the observation space. For example, one can define the design matrix following the approach used to define the covariance weighting kernels in [8]. In fact, this formulation has some similarity with spatial covariance localization widely used in the numerical weather prediction applications to remove spurious correlations in ensemble-based prior covariance matrices. Conversely, here we define a design matrix \mathbf{W} to weight/localize covariances between observational sensors based on their respective contribution to the uncertainty of the inversion parameter. If one believes that the effect of correlation on the design should decay in space or in the presence of spurious correlations in observation errors, one can encode this decay in the definition of the weighting function ϖ , in other words, the entries of the design matrix \mathbf{W} . This formulation will enable us to fix the size of the design space to that of the observation space, even when spatiotemporal correlations are considered, thus reducing the computational cost of solving the OED optimization problem.

If the problem is time independent, the matrix $\mathbf{\Gamma}_{\text{noise}}$ describes the covariances between errors of pairs of candidate sensors. In this case the weighting kernel \mathbf{W} requires a weighting function that depends only on pairs of design variables, that is, $\varpi := \omega(\zeta_i, \zeta_j)$; and the weighting kernel, described by its respective entries, takes the form $\mathbf{W} = [\omega(\zeta_i, \zeta_j)]_{i,j=1,2,\dots,n_s}$.

Similarly, if the problem is time dependent, while only space correlations are considered, the weight function $\varpi(t_m, t_n; \zeta_i, \zeta_j)$ vanishes for any two different time instances $t_m \neq t_n$, and the weighting kernel becomes a block diagonal matrix taking the form $\mathbf{W} = \bigoplus_{m=1}^{n_t} ([\omega(\zeta_i, \zeta_j)]_{i,j=1,2,\dots,n_s})$.

In general, the design weighting function $\omega(\zeta_i, \zeta_j)$ must be symmetric, differentiable, and with range $\subseteq [0, +\infty)$. Moreover, we would prefer a weighting function with range $[0, 1]$, which inherently promotes a binary design. Further discussion about the spatial weighting function ω is given in [Subsection 3.2](#), with other candidate weighting functions discussed in [Appendix A](#).

3.2. On the choice of the weighting function. The value of the weighting function at any pair of observation gridpoints (and design variables) is used to localize the effect of the correlation between any pair of points. Specifically, $\omega(\zeta_i, \zeta_j)$ scales the (i, j) th entry of the spatial observation error covariance matrix $\mathbf{\Gamma}_{\text{noise}}$. Moreover, if $i = j$, then the weighting value scales the uncertainty level of the i th candidate sensor location. We regard the weighting value here in the general sense as a value that indicates the relative importance of each candidate sensor. The least requirement of the weighting function ω is to be differentiable—this is required to formulate the gradient of the optimality criterion with respect to the design—with the range $\subseteq [0, +\infty)$, and to satisfy the following:

$$(3.5) \quad \omega(\zeta_i, \zeta_j) \geq 0, \quad \forall i \neq j; \quad \omega(\zeta_i, \zeta_j) > 0, \quad \forall i = j; \quad i, j = 1, 2, \dots, n_s.$$

Ideally one would prefer a weighting function ω with a range $[0, 1]$, which simplifies the interpretability of the solution of the OED problem. Moreover, in order to control the sparsity of the design, in the optimization problem (2.8) the penalty function $\Phi(\cdot)$ is employed. Assuming, for example, that an ℓ_p norm is used, we define the penalty function as

$$(3.6) \quad \Phi(\zeta) := \left\| \left(\omega(\zeta_1, \zeta_1), \omega(\zeta_2, \zeta_2), \dots, \omega(\zeta_{n_s}, \zeta_{n_s}) \right)^\top \right\|_p,$$

where the penalty is asserted on the results of the weighting function, regardless of the domain of the design variables themselves. The reason is that the role of the penalty function is to limit the magnitude of the weights associated with the uncertainty level of each candidate sensor location.

An example of such a function is the square root (SQRT) kernel defined as

$$(3.7) \quad \omega(\zeta_i, \zeta_j) = \sqrt{\zeta_i} \sqrt{\zeta_j}; \quad \frac{\partial \omega(\zeta_i, \zeta_j)}{\partial \zeta_k} = \frac{1}{2} \left(\frac{\sqrt{\zeta_j}}{\sqrt{\zeta_i}} \delta_{i,k} + \frac{\sqrt{\zeta_i}}{\sqrt{\zeta_j}} \delta_{j,k} \right),$$

where $\zeta_i, \zeta_j \in [0, 1]$; $i, j = 1, 2, \dots, n_s$, and $\delta_{i,k}$ is the Kronecker delta function. However, this requires restricting the domain of the design variables ζ_i, ζ_j to $[0, 1]$ and would require adding box constraints to the optimization problem. We will show later that this choice of the weighting function (3.7) coincides with the traditional OED formulation. Another candidate weighting function is the following exponential (EXP) function:

$$(3.8) \quad \omega(\zeta_i, \zeta_j) = e^{-a(\zeta_i + \zeta_j)}; \quad \frac{\partial \omega(\zeta_i, \zeta_j)}{\partial \zeta_k} = -a(\delta_{i,k} + \delta_{j,k}) \omega(\zeta_i, \zeta_j)$$

where $\zeta_i, \zeta_j \in (-\infty, \infty)$; $i, j = 1, 2, \dots, n_s$, and $a \geq 1$ is a positive scaling coefficient. This function yields nonnegative weights; however, the weights are not limited to the interval $[0, 1]$ and thus should be scaled properly after solving the optimization problem.

An ideal weighting kernel should help obtain a binary solution. This can be achieved by choosing a function that promotes values closer to the bounds of its range. To this end one can, for example, use a sigmoid kernel. A sigmoid weighting function can take, for example, the following forms (3.9a, 3.9b) respectively:

$$(3.9a) \quad \omega(\zeta_i, \zeta_j) = (1 + \exp(-a\zeta_i \zeta_j))^{-1}; \quad \frac{\partial \omega(\zeta_i, \zeta_j)}{\partial \zeta_k} = a(\delta_{i,k} \zeta_j + \delta_{j,k} \zeta_i) \omega(\zeta_i, \zeta_j) (1 - \omega(\zeta_i, \zeta_j)),$$

$$(3.9b) \quad \omega(\zeta_i, \zeta_j) = \left(1 + \exp\left(-a \frac{\zeta_i + \zeta_j}{2}\right) \right)^{-1}; \quad \frac{\partial \omega(\zeta_i, \zeta_j)}{\partial \zeta_k} = \frac{a(\delta_{i,k} + \delta_{j,k})}{2} \omega(\zeta_i, \zeta_j) (1 - \omega(\zeta_i, \zeta_j)),$$

where $\zeta_i, \zeta_j \in (-\infty, \infty)$; $i, j = 1, 2, \dots, n_s$, and $a \geq 1$ is a positive scaling coefficient. We generally set the scaling coefficient $a = 1$, unless otherwise stated explicitly. In this case the value of the design itself is not constrained, but the resulting weights applied to the inverse observation correlations are inherently restricted to the interval $[0, 1]$. This approach enables using unconstrained optimization routines to solve the OED optimization problem.

In the remainder of [Section 3](#), we will keep the discussion independent from the specific choice of the design weighting function ω and will discuss two cases. In the first case the observation error covariance matrix is block diagonal with only space correlations ([Subsection 3.3](#)), and in the second case both space and time correlations are allowed ([Subsection 3.4](#)).

3.3. Space correlations. Let $\zeta \in \Xi \subseteq \mathbb{R}^{n_s}$ be the design, and assume that the observation errors are temporally uncorrelated. In this case, as discussed in [Subsection 3.1](#), the observation error covariance matrix and the design weighting matrix take the form

$$(3.10) \quad \mathbf{\Gamma}_{\text{noise}} = \bigoplus_{m=1}^{n_t} (\mathbf{R}_m); \quad \mathbf{W} = \bigoplus_{m=1}^{n_t} \left(\sum_{i,j=1}^{n_s} \omega(\zeta_i, \zeta_j) \mathbf{e}_i \mathbf{e}_j^\top \right),$$

where \mathbf{e}_i is the i th versor of \mathbb{R}^{n_s} , that is, the i th vector in the natural basis. In this case the derivative of \mathbf{W} with respect to a given entry of the design vector, ζ_j , is a sparse symmetric matrix with only nonzero entries in the j th row and the j th column of each block. Specifically, if we define the vector of partial derivatives of weights

$$(3.11) \quad \eta_j = \left(\frac{1}{1+\delta_{1,j}} \frac{\partial \omega(\zeta_1, \zeta_j)}{\partial \zeta_j}, \frac{1}{1+\delta_{2,j}} \frac{\partial \omega(\zeta_2, \zeta_j)}{\partial \zeta_j}, \dots, \frac{1}{1+\delta_{n_s,j}} \frac{\partial \omega(\zeta_{n_s}, \zeta_j)}{\partial \zeta_j} \right)^\top,$$

then it immediately follows that $\frac{\partial \mathbf{W}}{\partial \zeta_j} = \mathbf{e}_j \eta_j^\top + \eta_j \mathbf{e}_j^\top$; hence, by utilizing the distributive property of the Hadamard product and the fact that \mathbf{R}_m is symmetric and $\mathbf{R}_k \odot (\eta_j \mathbf{e}_j^\top) = ((\mathbf{R}_k \mathbf{e}_j) \odot \eta_j) \mathbf{e}_j^\top$, it follows that

$$(3.12) \quad \frac{\partial \mathbf{W}_\Gamma(\zeta)}{\partial \zeta_j} = -\mathbf{W}_\Gamma(\zeta) \bigoplus_{m=1}^{n_t} \left(\mathbf{e}_j ((\mathbf{R}_m \mathbf{e}_j) \odot \eta_j)^\top + ((\mathbf{R}_m \mathbf{e}_j) \odot \eta_j) \mathbf{e}_j^\top \right) \mathbf{W}_\Gamma(\zeta).$$

From [\(3.2\)](#), it follows that

$$(3.13) \quad \begin{aligned} \mathbf{W}_\Gamma(\zeta) &= \bigoplus_{m=1}^{n_t} (\mathbf{V}_m^\dagger(\zeta)), \quad \mathbf{L} = \bigoplus_{m=1}^{n_t} (\mathbf{L}_m), \\ \mathbf{V}_m^\dagger(\zeta) &:= \mathbf{L}_m^\top \mathbf{V}_m^{-1}(\zeta) \mathbf{L}_m, \quad \mathbf{V}_m(\zeta) := \mathbf{L}_m \left(\mathbf{R}_m \odot \left(\sum_{i,j=1}^{n_s} \omega(\zeta_i, \zeta_j) \mathbf{e}_i \mathbf{e}_j^\top \right) \right) \mathbf{L}_m^\top, \end{aligned}$$

where the blocks of the matrix \mathbf{L} , \mathbf{L}_m extract the rows/columns from \mathbf{R}_m corresponding to active sensors and are all equal; that is, $\mathbf{L}_i = \mathbf{L}_j \forall i, j = 1, \dots, n_t$. Given the general form of the derivative [\(2.9\)](#), the gradients of the A- and D-optimality criteria [\(2.5\)](#), in the case of temporally uncorrelated observation errors, take the following respective forms (detailed derivation is given

in [Appendix B.1](#), [Appendix C.1](#)):

$$(3.14a) \quad \nabla_{\zeta} \Psi^{\text{GA}}(\zeta) = 2 \sum_{m=1}^{n_t} \text{diag} \left(\mathbf{V}_m^{\dagger}(\zeta) \mathbf{F}_{0,m} \mathbf{H}^{-1}(\zeta) \mathbf{P}^* \mathbf{P} \mathbf{H}^{-1}(\zeta) \mathbf{F}_{m,0}^* \mathbf{V}_m^{\dagger}(\zeta) (\mathbf{R}_m \odot \mathbf{W}') \right),$$

$$(3.14b) \quad \nabla_{\zeta} \Psi^{\text{GD}}(\zeta) = 2 \sum_{m=1}^{n_t} \text{diag} \left(\mathbf{V}_m^{\dagger}(\zeta) \mathbf{F}_{0,m} \mathbf{H}^{-1}(\zeta) \mathbf{P}^* \Sigma_{\text{post}}^{-1}(\zeta) \mathbf{P} \mathbf{H}^{-1}(\zeta) \mathbf{F}_{m,0}^* \mathbf{V}_m^{\dagger}(\zeta) (\mathbf{R}_m \odot \mathbf{W}') \right),$$

where $\mathbf{F}_{m,0}^*$ is the adjoint of $\mathbf{F}_{0,m}$, and \mathbf{W}' is a matrix with columns set by using [\(3.11\)](#); that is,

$$(3.15) \quad \mathbf{W}' = [\eta_1, \eta_2, \dots, \eta_{n_s}].$$

If we assume a diagonal observational error covariance matrix $\mathbf{\Gamma}_{\text{noise}}$ and utilize the SQRT kernel [\(3.7\)](#), then the matrix of the derivative reduces to $\mathbf{W}' = \frac{1}{2} \mathbf{I}$. In this case the gradient of the A-optimality criterion [\(3.14a\)](#) and the gradient of the D-optimality criterion [\(3.14a\)](#), respectively, reduce to

$$(3.16a) \quad \nabla_{\zeta} \Psi^{\text{GA}}(\zeta) = \sum_{m=1}^{n_t} \sum_{i=1}^{N_{\text{goal}}} \mathbf{s}_{i,m} \odot \mathbf{s}_{i,m}; \quad \nabla_{\zeta} \Psi^{\text{GD}}(\zeta) = \sum_{m=1}^{n_t} \sum_{i=1}^{N_{\text{goal}}} \tilde{\mathbf{s}}_{i,m} \odot \tilde{\mathbf{s}}_{i,m},$$

$$(3.16b) \quad \mathbf{s}_{i,m} := \mathbf{L}_m^{\top} \left(\mathbf{L}_m \text{diag}(\zeta) \mathbf{R}_m^{\frac{1}{2}} \mathbf{L}_m^{\top} \right)^{-1} \mathbf{L}_m \mathbf{F}_{0,m} \mathbf{H}^{-1}(\zeta) \mathbf{P}^* \mathbf{e}_i,$$

$$(3.16c) \quad \tilde{\mathbf{s}}_{i,m} := \mathbf{L}_m^{\top} \left(\mathbf{L}_m \text{diag}(\zeta) \mathbf{R}_m^{\frac{1}{2}} \mathbf{L}_m^{\top} \right)^{-1} \mathbf{L}_m \mathbf{F}_{0,m} \mathbf{H}^{-1}(\zeta) \mathbf{P}^* \Sigma_{\text{post}}^{-\frac{1}{2}}(\zeta) \mathbf{e}_i,$$

where we utilized the following [Lemma 3.1](#), which can be proven with elementary linear algebra.

LEMMA 3.1. *Given a symmetric matrix \mathbf{A} and a nonnegative diagonal matrix \mathbf{B} such that $\mathbf{A}, \mathbf{B} \in \mathbb{R}^{n \times n}$, then $\text{diag}(\mathbf{A} \mathbf{A}^{\top} \mathbf{B}) = \text{diag}(\mathbf{B}^{\frac{1}{2}} \mathbf{A} \mathbf{B}^{\frac{1}{2}}) = \sum_{i=1}^n \mathbf{s}_i \odot \mathbf{s}_i$; where $\mathbf{s}_i = \mathbf{B}^{\frac{1}{2}} \mathbf{A} \mathbf{e}_i$.*

Note that by utilizing the SQRT kernel [\(3.7\)](#), that is, by setting $\omega(\zeta_i, \zeta_j) := \sqrt{\zeta_i \zeta_j}$, we retrieve the standard OED formulation

$$(3.17) \quad \mathbf{W}_{\Gamma} = \bigoplus_{m=1}^{n_t} \left(\mathbf{L}_m^{\top} \left(\mathbf{L}_m \text{diag}(\sqrt{\zeta})^{\top} \mathbf{R}_m \text{diag}(\sqrt{\zeta}) \mathbf{L}_m^{\top} \right)^{-1} \mathbf{L}_m \right),$$

where $\sqrt{\zeta} = (\sqrt{\zeta_1}, \sqrt{\zeta_2}, \dots, \sqrt{\zeta_{n_s}})^{\top}$, where \mathbf{R}_m are diagonal. This shows that the traditional OED formulation is equivalent to applying a Hadamard product weighting kernel to the observation covariance matrix. Specifically, the variance of the observation error associated with the i th candidate sensor location is weighted by the value of the corresponding design ζ_i . In this case the design variables are the weights themselves, and the weights must be bounded in the interval $[0, 1]$, which is normal in the traditional OED formulation.

Generally speaking, the proposed formulation reduces to the standard OED approach only if the observation errors are uncorrelated and the symmetric kernel function utilized is separable, that is, $\omega(\zeta_i, \zeta_j) = g(\zeta_i)g(\zeta_j)$ for some function $g_*(\zeta_*) : \Omega \subseteq \mathbb{R} \rightarrow [0, \infty]$. In this case, the weighted precision matrix can be written as

$$\mathbf{W}_{\Gamma} = \left(\text{diag}(g(\zeta_1), g(\zeta_2), \dots, g(\zeta_{n_s})) \mathbf{\Gamma}_{\text{noise}} \text{diag}(g(\zeta_1), g(\zeta_2), \dots, g(\zeta_{n_s})) \right)^{-1}.$$

However, this cannot be done for inseparable kernels such as [\(3.9\)](#), which sets the new formulation based on the Hadamard product more general than the traditional formulation of the OED problem.

3.4. Spatiotemporal correlations. In time-dependent problems, when the observation errors are temporally correlated, the observation noise covariance $\mathbf{\Gamma}_{\text{noise}}$ is a full symmetric matrix, with blocks \mathbf{R}_{mn} representing cross-covariances between observation errors at time instances t_n and t_m , respectively. In space-time settings, one can associate a design variable $\zeta_{i,m}$ for the i th candidate sensor, from n_s candidate locations, at time instance t_m . In this case, however, the design space $\mathbb{R}^{n_s \times n_t}$ grows with the number of observation time instances n_t , and the decision-making process (e.g., thresholding) will be harder to carry out or even interpret. An alternative approach is to associate a design variable ζ_i with the i th candidate sensor location, while controlling its effect in space and over time. For example, we can fix the design variable ζ_i over time, that is, $\zeta_i = \zeta_{i,m} \forall m = 1, 2, \dots, n_t$, while controlling its effect by using the form of ω and by introducing a temporal decorrelation function.

In the majority of time-dependent applications, the temporal correlation strength generally decays in time. In some applications, the correlation between distant temporal points is dominated by spurious correlations, and their effect on the design should be damped out. In this case, in order to choose an optimal design, the temporal effect of a design weight for a candidate sensor location should also decay in time to damp down the effect of spurious correlations on the design selection. For example, one could use the weighting function $\varpi := \rho(t_m, t_n) \omega(\cdot)$, to weight the entries of \mathbf{R}_{mn} , where, as before, $\omega(\cdot)$ is a space weighting function and $\rho(t_m, t_n)$ is a symmetric function such that $\rho(t_m, t_m) = 1$ and is conversely related with the distance between t_m and t_n . In this case the entries of $\mathbf{\Gamma}_{\text{noise}}$ are weighted by

$$(3.18) \quad \varpi(\zeta_i, \zeta_j; t_m, t_n) := \rho(t_m, t_n) \omega(\zeta_i, \zeta_j); \quad \begin{array}{l} i, j = 1, 2, \dots, n_s, \\ m, n = 1, 2, \dots, n_t. \end{array}$$

One could use a Gaussian-like decorrelation function

$$(3.19) \quad \rho(t_m, t_n) := \exp(-d(t_m, t_n)/2\ell^2),$$

where $d(t_m, t_n)$ is a distance function between time instances t_m and t_n and where ℓ is a predefined temporal-correlation length scale. An alternative choice of the weighting coefficients is to employ the fifth-order piecewise-rational function (3.20) of Gaspari and Cohn [21]:

$$(3.20) \quad \rho(t_m, t_n) = \begin{cases} -\frac{v^5}{4} + \frac{v^4}{2} + \frac{5v^3}{8} - \frac{5v^2}{3} + 1, & 0 \leq v \leq 1 \\ \frac{v^5}{12} - \frac{v^4}{2} + \frac{5v^3}{8} + \frac{5v^2}{3} - 5v + 4 - \frac{2}{3v}, & 1 \leq v \leq 2 \\ 0, & 2 \leq v, \end{cases}$$

where $v := \frac{d(t_m, t_n)}{\ell}$ and, as before, ℓ is a predefined correlation length scale and $d(t_m, t_n)$ measures the temporal distance between time instances t_m, t_n . The simplest choice of such a temporal distance function is the Euclidean distance defined as $d(t_m, t_n) := |t_m - t_n|$. Note that the parameter ℓ here controls the speed at which the decorrelation decays over time, and this should be application specific. The function (3.20) is designed to have compact support such that it is nonzero only for a small local region and zero everywhere else and is used for covariance localization in the data assimilation context; see, for example, [25, 47, 8, 31].

Note that this function is independent from the design variable ζ and is introduced for flexibility, for example, to damp out spurious correlations. One can simply choose $\rho(t_m, t_n) = 1$ if the observation error correlations are correctly specified at all scales. The discussion below is independent from the choice of the temporal weighting function ρ .

In space-time settings, the weighted version of the space-time observation error precision matrix takes the form $\mathbf{W}_\Gamma = \mathbf{L}^\top (\mathbf{L} (\boldsymbol{\Gamma}_{\text{noise}} \odot \mathbf{W}) \mathbf{L}^\top)^{-1} \mathbf{L}$, with the space-time weighting matrix \mathbf{W} defined, elementwise, as

$$(3.21) \quad \mathbf{W} := \left[\varpi \left(\zeta_{(k-1) \bmod n_s + 1}, \zeta_{(h-1) \bmod n_s + 1}; t_{\lfloor \frac{k-1}{n_t} \rfloor + 1}, t_{\lfloor \frac{h-1}{n_t} \rfloor + 1} \right) \right]_{k,h=1,2,\dots,N_{\text{obs}}},$$

where $\lfloor \cdot \rfloor$ is the floor operation and \bmod represents the modulo operation. Note that the entrywise representation of the weighting kernel (3.21) shows that the design variables are time independent.

The derivative of the optimality criterion, required for the gradient-based solution of the OED problem, follows directly once the matrix derivative of the weight matrix \mathbf{W} in (3.21) is formulated. To this end, let us define the vector of partial derivatives $\vartheta_{k,n} \in \mathbb{R}^{N_{\text{obs}}}$, $N_{\text{obs}} = n_s \times n_t$, with the k th entry denoted as $\vartheta_{i,m}[k]$ and given by

$$(3.22) \quad \vartheta_{i,m}[k] := \frac{1}{1 + \delta_{i,(k-1) \bmod n_s + 1}} \frac{\partial}{\partial \zeta_i} \varpi \left(\zeta_i, \zeta_{(k-1) \bmod n_s + 1}; t_m, t_{\lfloor \frac{k-1}{n_t} \rfloor + 1} \right); \quad \begin{array}{l} i = 1, \dots, n_s, \\ m = 1, \dots, n_t, \\ k = 1, \dots, N_{\text{obs}}. \end{array}$$

The partial derivative of the weight matrix \mathbf{W} with respect to the design variable ζ_i is a symmetric matrix given by

$$(3.23) \quad \frac{\partial \mathbf{W}}{\partial \zeta_i} = \sum_{m=1}^{n_t} \mathbf{e}_q \vartheta_{i,m}^\top + \sum_{m=1}^{n_t} \vartheta_{i,m} \mathbf{e}_q^\top, \quad q = i + (m-1)n_s; \quad i = 1, 2, \dots, n_s,$$

where \mathbf{e}_q here is the q th natural basis vector in $\mathbb{R}^{N_{\text{obs}}}$. By applying the distributive property of the Hadamard product, the partial derivatives of the weighted precision matrix take the form

$$(3.24) \quad \frac{\partial \mathbf{W}_\Gamma}{\partial \zeta_i} = -\mathbf{W}_\Gamma(\zeta) \left(\sum_{m=1}^{n_t} \mathbf{e}_q ((\boldsymbol{\Gamma}_{\text{noise}}^{-1} \mathbf{e}_q) \odot \vartheta_{i,m})^\top + \sum_{m=1}^{n_t} ((\boldsymbol{\Gamma}_{\text{noise}}^{-1} \mathbf{e}_q) \odot \vartheta_{i,m}) \mathbf{e}_q^\top \right) \mathbf{W}_\Gamma(\zeta).$$

Given (3.24, 3.22) and, as shown in (Appendix B.2, Appendix C.2), in the presence of spatiotemporal observation correlations, the gradient of the A- and D-optimality criteria take the following respective forms:

(3.25a)

$$\nabla_\zeta \Psi^{\text{GA}}(\zeta) = 2 \sum_{i=1}^{n_s} \sum_{m=1}^{n_t} \mathbf{e}_i \mathbf{e}_q^\top \mathbf{W}_\Gamma(\zeta) \mathbf{F} \mathbf{H}^{-1}(\zeta) \mathbf{P}^* \mathbf{P} \mathbf{H}^{-1}(\zeta) \mathbf{F}^* \mathbf{W}_\Gamma(\zeta) ((\boldsymbol{\Gamma}_{\text{noise}}^{-1} \mathbf{e}_q) \odot \vartheta_{i,m}),$$

$$(3.25b) \quad \nabla_\zeta \Psi^{\text{GD}}(\zeta) = 2 \sum_{i=1}^{n_s} \sum_{m=1}^{n_t} \mathbf{e}_i (\boldsymbol{\Gamma}_{\text{noise}}^{-1} \mathbf{e}_q \odot \vartheta_{i,m})^\top \mathbf{W}_\Gamma(\zeta) \mathbf{F} \mathbf{H}^{-1}(\zeta) \mathbf{P}^* \boldsymbol{\Sigma}_{\text{post}}^{-1}(\zeta) \mathbf{P} \mathbf{H}^{-1}(\zeta) \mathbf{F}^* \mathbf{W}_\Gamma(\zeta) \mathbf{e}_q.$$

3.5. Computational considerations. The OED objective function and the associated gradient together form the main bottleneck in the process of an OED optimization problem. Evaluating the objective function \mathcal{T} of the OED optimization problem (2.8) and the associated gradient requires evaluating the optimality criterion Ψ and the associated gradient. They also require specifying the

penalty function Φ . The cost of evaluating the penalty function and the associated gradient, with respect to the design parameter, however, is negligible compared with the cost of evaluating Ψ and the associated gradient. Thus, in what follows we focus on the cost of the A-optimality criterion and the associated gradient in terms of the number of forward model evaluations. The analysis extends easily to other optimality criteria including D-optimality.

For simplicity, we assume that the prediction operator \mathbf{P} and the corresponding adjoint \mathbf{P}^* each require one forward model evaluation. The A-optimality criterion $\zeta^{\text{A-opt}}$ described by (2.5) requires one Hessian solve, a forward, and an adjoint integration of the model \mathbf{F} for each entry of the posterior covariance matrix diagonal. The Hessian, being the inverse of the posterior covariance of the model parameter θ , is a function of the relaxed design; see, for example, [7] for details.

A preconditioned conjugate gradient (CG) method is used for Hessian solves, which requires a forward and an adjoint model evaluation for each application of the Hessian. We use the prior covariance as a preconditioner. In this case, and by assuming the numerical rank of the prior preconditioned data misfit Hessian [13] is $r \ll N_{\text{state}}$, then one Hessian solve costs $\mathcal{O}(r)$ CG iterations, that is, $\mathcal{O}(2r)$ forward model evaluations. Thus, one evaluation of the objective function \mathcal{T} in (2.8), assuming A-optimality, costs $\mathcal{O}(2r N_{\text{goal}} + 2 N_{\text{goal}}) = \mathcal{O}(2r N_{\text{goal}})$ forward model solves.

In the case of space correlations, evaluating the gradient of the A-optimality criterion, as described by (3.16a), requires one Hessian solve and two applications of the forward model (including one evaluation of the prediction operator) for each vector in the natural basis $\mathbb{R}^{N_{\text{goal}}}$ at each time instance. Thus, the cost of evaluating the gradient $\nabla_{\zeta} \Psi^{\text{GA}}(\zeta)$ is $\mathcal{O}(2r n_t N_{\text{goal}} + 2 n_t N_{\text{goal}}) = \mathcal{O}(r n_t N_{\text{goal}})$. Similarly, in the case of spatiotemporal correlations, evaluating the gradient (3.25a) costs $\mathcal{O}(n_s n_t (4r + 4)) = \mathcal{O}(4r n_t n_s)$ evaluations of the forward model \mathbf{F} .

3.6. Efficient computation of OED objective and gradient. Solving the OED optimization problem requires repeated evaluation of the trace of the posterior covariance matrix. Moreover, as discussed in Subsection 3.5, constructing the gradient of the optimality criterion requires many forward and backward evaluations of the numerical model, with the computational cost dominated by the cost of evaluating the Hessian matrix \mathbf{H} . To reduce the computational cost, we approximate the Hessian by a randomized approximation of the eigenvalues of a Hermitian matrix as described in [40]; see Appendix D.1 for details. Note that the Hessian matrix \mathbf{H} is never constructed in practice; alternatively, only the effect of its inverse on a vector $\mathbf{H}^{-1}\mathbf{x}$ is required.

Here we discuss using randomized approaches to approximate the optimality criterion for efficient calculation of both the objective and its gradient. Specifically, we utilize a randomized approximation of the matrix trace for A-optimal designs, and we defer the discussion of randomized approximation of the D-optimality criterion to future work.

Given a covariance matrix \mathbf{C} , one can estimate its trace following a Monte Carlo approach, using the relation $\text{Tr}(\mathbf{C}) = \mathbb{E}[\mathbf{z}^T \mathbf{C} \mathbf{z}] \approx \sum_{r=1}^{n_r} \mathbf{z}_r^T \mathbf{C} \mathbf{z}_r$, where $\{\mathbf{z}_r\}_{r=1,2,\dots,n_r}$ are sampled from the distribution of \mathbf{z} , which is generally an i.i.d. random variable that follows a specific probability distribution. The most commonly used are Gaussian and Rademacher distributions [11]. The development of the criterion below is independent from the choice of the probability distribution. In the numerical experiments, however, we resort to the Hutchinson trace estimator where the samples \mathbf{z}_i are drawn from the Rademacher distribution.

An approximate A-optimality criterion $\tilde{\Psi}^{\text{GA}}(\zeta) \approx \Psi^{\text{GA}}(\zeta)$ takes the form

$$(3.26) \quad \tilde{\Psi}^{\text{GA}}(\zeta) = \frac{1}{n_r} \sum_{r=1}^{n_r} \mathbf{z}_r^T \Sigma_{\text{post}}(\zeta) \mathbf{z}_r = \frac{1}{n_r} \sum_{r=1}^{n_r} \mathbf{z}_r^T \mathbf{P} (\mathbf{F} \mathbf{W}_\Gamma(\zeta) \mathbf{F}^* + \mathbf{\Gamma}_{\text{pr}}^{-1})^{-1} \mathbf{P}^* \mathbf{z}_r,$$

with $\mathbf{z}_r \in \mathbb{R}^{N_{\text{goal}}}$, and $\mathbf{W}_\Gamma(\zeta)$ is given by (3.2). The derivative of this randomized A-optimality criterion with respect to the i th design variable, where $i = 1, 2, \dots, n_s$, is

$$(3.27) \quad \frac{\partial \tilde{\Psi}^{\text{GA}}(\zeta)}{\partial \zeta_i} = \frac{1}{n_r} \sum_{r=1}^{n_r} \mathbf{z}_r^T \mathbf{P} \mathbf{H}^{-1}(\zeta) \mathbf{F}^* \mathbf{W}_\Gamma(\zeta) \left(\mathbf{\Gamma}_{\text{noise}} \odot \frac{\partial \mathbf{W}(\zeta)}{\partial \zeta_i} \right) \mathbf{W}_\Gamma(\zeta) \mathbf{F} \mathbf{H}^{-1}(\zeta) \mathbf{P}^* \mathbf{z}_r.$$

If we assume that the observations are temporally uncorrelated, the gradient takes the form (see Appendix B.3 for details)

$$(3.28) \quad \nabla_\zeta \tilde{\Psi}^{\text{GA}}(\zeta) = \frac{2}{n_r} \sum_{r=1}^{n_r} \sum_{m=1}^{n_t} \psi_{r,m}^* \odot ((\mathbf{R}_m \odot \mathbf{W}') \psi_{r,m}); \quad \begin{aligned} \psi_{r,m} &:= \mathbf{V}_m^\dagger(\zeta) \mathbf{F}_{0,m} \mathbf{H}^{-1}(\zeta) \mathbf{P}^* \mathbf{z}_r, \\ \psi_{r,m}^* &:= (\mathbf{z}_r^T \mathbf{P} \mathbf{H}^{-1}(\zeta) \mathbf{F}_{m,0}^* \mathbf{V}_m^\dagger(\zeta))^T. \end{aligned}$$

In the presence of spatiotemporal correlations, the gradient is (see Appendix B.3)

$$(3.29) \quad \nabla_\zeta \tilde{\Psi}^{\text{GA}}(\zeta) = 2 \sum_{r=1}^{n_r} \sum_{i=1}^{n_s} \sum_{m=1}^{n_t} \mathbf{e}_i \psi_r^* \mathbf{e}_q ((\mathbf{\Gamma}_{\text{noise}} \mathbf{e}_q) \odot \vartheta_{i,m})^T \psi_r; \quad \begin{aligned} \psi_r &:= \mathbf{W}_\Gamma(\zeta) \mathbf{F} \mathbf{H}^{-1}(\zeta) \mathbf{P}^* \mathbf{z}_r, \\ \psi_r^* &:= \mathbf{z}_r^T \mathbf{P} \mathbf{H}^{-1}(\zeta) \mathbf{F}^* \mathbf{W}_\Gamma(\zeta). \end{aligned}$$

4. Numerical Experiments. We use an advection-diffusion model to simulate the transport of a contaminant field $u(\mathbf{x}, t)$ in a closed domain \mathcal{D} . A set of candidate sensor locations are predefined, at which the contaminant is to be measured at specific locations in the domain at predefined time instances. The end goal is to predict the concentration of the contaminant at a future time instance, beyond the simulation time. To achieve this goal, first we need to find the *optimal* subset of sensors, from the candidate locations, to deploy a small number of sensors. Here, we define optimality in the sense of A-optimal designs.

4.1. Problem setup. In this section, we describe in detail the setup of the numerical experiments carried out in this work.

4.1.1. Model: advection-diffusion. The governing equation of the contaminant $u(\mathbf{x}, t)$ is

$$(4.1) \quad \begin{aligned} u_t - \kappa \Delta u + \mathbf{v} \cdot \nabla u &= 0 & \text{in } \mathcal{D} \times [0, T], \\ u(x, 0) &= \theta & \text{in } \mathcal{D}, \\ \kappa \nabla u \cdot \mathbf{n} &= 0 & \text{on } \partial \mathcal{D} \times [0, T], \end{aligned}$$

where $\kappa > 0$ is the diffusivity, T is the simulation final time, and \mathbf{v} is the velocity field. The domain \mathcal{D} , sketched in Figure 1(left), is the region $(0, 1) \times (0, 1)$, where the rectangular regions model two buildings $\mathbf{B}_1, \mathbf{B}_2$, respectively. The interior of these rectangular regions is excluded from the domain \mathcal{D} , and the contaminant is not allowed to enter. The boundary $\partial \mathcal{D}$ includes both the external boundary and the building walls. The velocity field \mathbf{v} is obtained by solving a steady Navier–Stokes equation, with the side walls driving the flow, as detailed in [36], and is shown in Figure 1(middle). We consider $\kappa > 0$ and \mathbf{v} to be known exactly.

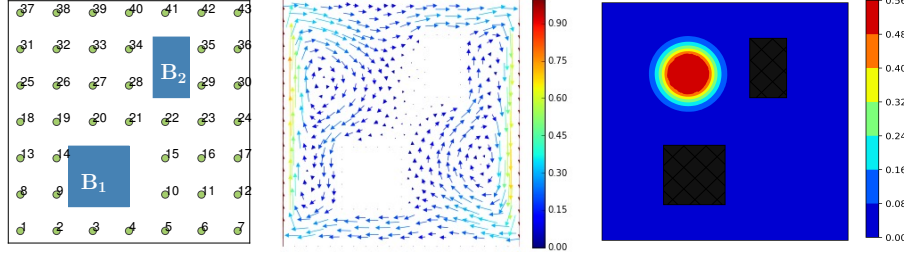


FIG. 1. Advection-diffusion model domain, candidate sensor locations, velocity field, and ground truth of the model parameter. Left: The physical domain \mathcal{D} , including outer boundary, and the two buildings B_1 , B_2 . The small circles indicate candidate sensor locations; the sensors are annotated based on their ordering in an observation vector. Middle: The velocity field is shown and is assumed to be fixed over time. Right: Ground truth of the model parameter, in other words, the true value of the model initial condition θ .

In this work we develop an implementation that utilizes the package HippyLib [46], which provides the forward operator \mathbf{F} , the adjoint \mathbf{F}^* , and a reduced-order Hessian approximation [4]; see Appendix D.1 for additional details on the reduced-order Hessian approximation. We follow the approach in [14], to discretize and simulate the flow PDE (4.1). Specifically, we use finite elements, with Lagrange triangular elements of order 2, with $N_{\text{state}} = 7863$ spatial degrees of freedom in space, and using implicit Euler for simulation in time. The true initial model parameter (shown in Figure 1(right)) is used to create a reference trajectory and synthetic observations.

4.1.2. Observations and observation noise. The contaminant is observed at a set of (candidate) observation gridpoints uniformly distributed in the space domain $\{\mathbf{x}_1, \dots, \mathbf{x}_{n_s}\} \subset \mathcal{D}$, at fixed time instances $\{t_1, t_2, \dots, t_{n_t}\} \subset [0, T]$. The candidate sensor locations, shown in Figure 1(left), constitute the observational grid, with $n_s = 43$ candidate sensor locations. The observation operator \mathcal{B}_k here is a restriction operator applied to the solution $u(\mathbf{x}, t)$ to extract solution values (i.e., concentration of the contaminant) at the predefined observation gridpoints at any time instance t_k . Here the observation times are $t_1 + s\Delta t$, with initial observation time $t_1 = 1$; $\Delta t = 0.2$ is the model simulation time step; and $s = 0, 1, \dots, 5$, resulting in $n_t = 6$ observation time instances. The matrix representation of the observation operator \mathcal{B}_k at any time instance t_k is plotted in Figure 2(left).

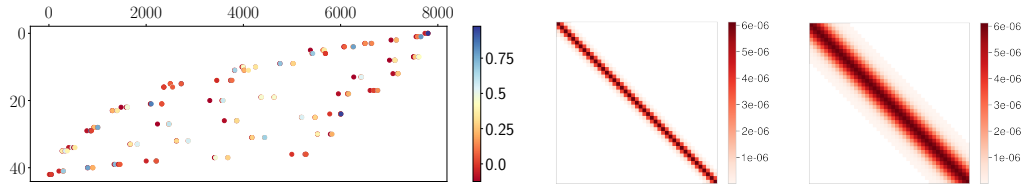


FIG. 2. Observation operator \mathcal{B}_k and observation error covariance matrix \mathbf{R}_k at any observation time instance t_k . To construct synthetic observation error covariances \mathbf{R}_k , we use a Gaspari-Cohn function (3.20) with a pre-defined length scale ℓ . Left: space observation operator \mathcal{B}_K . Middle: observation error covariance matrix \mathbf{R}_k with length scale of $\ell=1$. Right: observation error covariance matrix \mathbf{R}_k with length scale of $\ell=3$.

In the numerical experiments, we use synthetic observations and consider two cases of observation correlations. First, we assume that observations are uncorrelated, with fixed standard deviation $\sigma_{\text{obs}} = 2.475 \times 10^{-2}$. This value is obtained by considering a noise level of 5% of the maximum concentration of the contaminant at all observation points, found from a reference simulation, that is, the solution of (4.1), over the simulation timespan $[0, T]$, with the initial condition (Figure 1(right)). Second, we consider the case of space correlations where we run two sets of experiments with block diagonal covariance matrices, whose structure is shown in Figure 2. These are the covariances \mathbf{R}_k

between observation gridpoints at any observation time t_k and are constructed by using the fifth-order piecewise-rational function (3.20), with covariance length scales $\ell=1$, $\ell=3$, respectively. We use (3.20) to create correlations $\rho_{i,j}$ between i and j entries of the correlation matrix and scale it by observation noise variance σ_{obs}^2 to create a spatial covariance model, as shown in Figure 2. The row/column ordering of the covariance matrix corresponds to the entries of an observation vector; see Figure 1(left). The spatial covariance is stationary and is fixed over time; that is, $\mathbf{R}_k = \mathbf{R}$, $\forall k$.

4.1.3. Forward and adjoint operators. The forward operator \mathbf{F} is evaluated by solving (4.1) over the simulation timespan, and the observation operator is applied to the solution to extract solution values at the sensor locations at the predefined observation time instances. We use a space-time formulation where the model states at all simulation time points are stacked in one vector. A forward operator $\mathbf{F}_{0,k} \equiv \mathbf{F}_{t_0 \rightarrow t_k}$ maps the discretized model parameter θ to the measurements at observational gridpoints at time instance t_k . If we define $\mathcal{S}_{0,k} \equiv \mathcal{S}_{t_0 \rightarrow t_k}$ to be the solution operator over the interval $[t_0, t_k]$, and since \mathcal{B}_k is the observation operator at time instance t_k , then $\mathbf{F}_{0,k}\theta = \mathcal{B}_k\mathcal{S}_{0,k}\theta$. In the experiments here, we use the same observational grid at all time instances; that is, $\mathcal{B}_k = \mathcal{B}$, $\forall k$. Note that \mathcal{B} here is an interpolation operator from the model gridpoints to observational gridpoints.

A space-time observation vector is defined as $\mathbf{y} = [\mathbf{y}_1^\top, \mathbf{y}_2^\top, \dots, \mathbf{y}_{n_t}^\top]^\top$, where $\mathbf{y}_k \equiv \mathbf{y}[t_k]$ represents the sensor measurements at time instance t_k , with entries ordered as shown in Figure 1(left). The observation error covariance matrix $\mathbf{\Gamma}_{\text{noise}}$ is defined accordingly (see Subsection 2.4 for more details). Given this space-time formulation, we can rewrite the forward problem (2.1) as

$$(4.2) \quad [\mathbf{y}_1^\top, \mathbf{y}_2^\top, \dots, \mathbf{y}_{n_t}^\top]^\top = [(\mathbf{F}_{0,1}\theta)^\top, (\mathbf{F}_{0,2}\theta)^\top, \dots, (\mathbf{F}_{0,n_t}\theta)^\top]^\top + \delta, \quad \delta \sim \mathcal{N}(\mathbf{0}, \mathbf{\Gamma}_{\text{noise}}).$$

When the observation noise is temporally uncorrelated, the observation error covariance matrix $\mathbf{\Gamma}_{\text{noise}}$ is block diagonal, and the forward model can be written in the form

$$(4.3) \quad \mathbf{y}_k = \mathbf{F}_{0,k}\theta + \delta_k, \quad \delta_k \sim \mathcal{N}(\mathbf{0}, \mathbf{R}_k), \quad k = 1, 2, \dots, n_t.$$

This formulation (4.3) of the forward problem is advantageous for large-scale time-dependent problems because *checkpointing* is essential for scalability of the solution of both the Bayesian inverse problem and the OED. Forward and adjoint simulations scale efficiently by checkpointing the model solution at observation time instances t_k and by utilizing a model solution operator $\mathcal{S}_{k-1,k} \equiv \mathcal{S}_{t_{k-1} \rightarrow t_k}$ to propagate the model state over the simulation window $[t_{k-1}, t_k]$.

For a linear operator \mathbf{F} , the adjoint \mathbf{F}^* satisfies the property $\langle \mathbf{F}\mathbf{x}, \mathbf{y} \rangle = \langle \mathbf{x}, \mathbf{F}^*\mathbf{y} \rangle$, where \mathbf{x}, \mathbf{y} are elements of the space on which the product is defined. If \mathbf{F} is defined on the Euclidean space equipped with inner product $\langle \mathbf{x}, \mathbf{y} \rangle := \mathbf{x}^\top \mathbf{y}$, then the adjoint of the forward operator is equal to the matrix transpose of the discretized forward operator; that is, $\mathbf{F}^* = \mathbf{F}^\top$. However, here we use a finite-element discretization of the linear Bayesian inverse problem where the underlying infinite-dimensional problem is formulated on the space equipped $L^2(\mathcal{D})$ inner product. As explained in [14], the model adjoint is defined by using the Euclidean inner product weighted by the finite-element mass matrix \mathbf{M} . Specifically, for $\mathbf{u} \in \mathbb{R}^{N_\theta}$, $\mathbf{v} \in \mathbb{R}^{N_{\text{obs}}}$, it follows that $\langle \mathbf{F}\mathbf{u}, \mathbf{v} \rangle = (\mathbf{F}\mathbf{u})^\top \mathbf{v} = \mathbf{u}^\top \mathbf{F}^\top \mathbf{v} = \mathbf{u}^\top \mathbf{M} \mathbf{M}^{-1} \mathbf{F}^\top \mathbf{v} = \langle \mathbf{u}, \mathbf{M}^{-1} \mathbf{F}^\top \mathbf{v} \rangle_{\mathbf{M}}$, resulting in the model adjoint $\mathbf{F}^* = \mathbf{M}^{-1} \mathbf{F}^\top$. In the time-dependent settings utilized here, the adjoint takes the form $\mathbf{F}_{k,0}^* = \mathbf{M}^{-1} \mathcal{S}_{0,k}^\top \mathcal{B}_k^\top$.

4.1.4. Goal operator and its adjoint. The QoI γ is the value of contaminant concentration predicted around the second building \mathbf{B}_2 (see Figure 1) at a future time instance t_p , beyond the

simulation time. Specifically, we aim to predict the contaminant concentration withing a specific distance ϵ from the walls (i.e., boundary) of that building. For that, we set $\epsilon = 0.02$ and $t_p = 2.2$, which results in a prediction vector of size 138. If we define \mathbf{C}_p to be the matrix representation of a restriction operator that projects the solution at time t_p onto the prediction gridpoints (shown in Figure 3(left)), then the goal operator is defined as $\mathbf{P} = \mathbf{C}_p \mathbf{S}_{0,p}$. Since we are using finite-element discretization, the adjoint of the goal operator is defined as $\mathbf{P}^* = \mathbf{M}^{-1} \mathbf{S}_{0,p}^T \mathbf{C}_p^T$.

4.1.5. The prior. Following the setup in [7, 36], the prior distribution of the parameter θ is $\mathcal{N}(\theta_{\text{pr}}, \mathbf{\Gamma}_{\text{pr}})$, with $\mathbf{\Gamma}_{\text{pr}}$ being a discretization of \mathcal{A}^{-2} , where \mathcal{A} is a Laplacian operator. In particular, we use $\mathcal{A} = \delta I + \gamma \Theta \nabla$, where Θ is a symmetric positive definite tensor for anisotropic diffusion of the PDE (4.1), $\delta \gamma$ governs the variance of the prior samples, while the ratio $\frac{\gamma}{\delta}$ governs the correlation length scale [4, 46]. In our experiments, we set $\gamma = 1$ and $\delta = 16$. The ground truth and the prior QoI (shown in Figure 3(middle)) are obtained by applying the prediction operator \mathbf{P} to the true and the prior initial condition, respectively. That is, $\gamma_{\text{true}} = \mathbf{P} \theta_{\text{true}}$, and the goal QoI γ assumes a Gaussian prior $\mathcal{N}(\mathbf{P} \theta_{\text{pr}}, \mathbf{P} \mathbf{\Gamma}_{\text{pr}} \mathbf{P}^*)$. The prior covariance matrix of the goal QoI, that is, $\mathbf{P} \mathbf{\Gamma}_{\text{pr}} \mathbf{P}^*$, is displayed in Figure 3(right). The effect of the prior on the resulting design is an important issue; however, it is out of the scope of this work. Here we fix the prior across all experiments and focus on the performance due to observation covariance weighting.

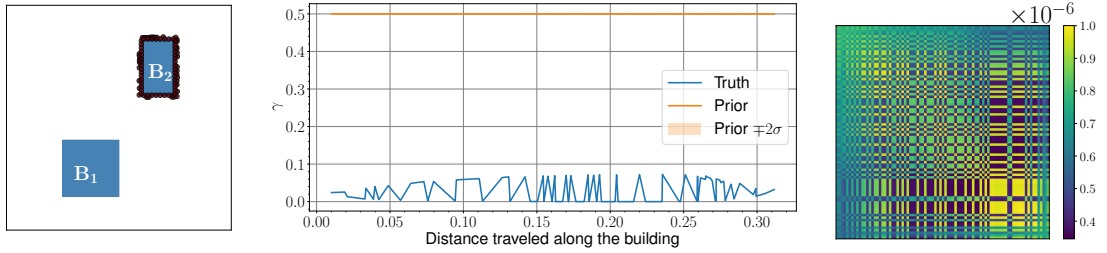


FIG. 3. *Left: gridpoints around the second building B_2 , at which the goal QoI γ is predicted. Middle: ground truth and the prior of the goal QoI γ . Here, the x-axis of the middle panel corresponds to the prediction gridpoints shown in the left panel reordered based on the distance traveled along the second building starting from the lower-left corner. Right: entries of the prior covariance matrix $\mathbf{P} \mathbf{\Gamma}_{\text{pr}} \mathbf{P}^*$, with rows/columns reordered to match the ordering on the x-axis of Figure 3(middle).*

In the numerical results discussed in Subsection 4.2, we will use γ_{True} to calculate an accuracy measure of the solution of an inverse problem. Specifically, we use the root-mean-squared error (RMSE) of QoI retrieved by Bayesian inversion γ defined as

$$(4.4) \quad \text{RMSE} := \frac{\|\gamma - \gamma_{\text{true}}\|_2}{\sqrt{N_{\text{goal}}}}.$$

4.1.6. OED regularization. We employ an ℓ_1 regularization term to induce a sparse design. Specifically, given the specific choice of the design weighting function ω , the regularization term and the associated derivative take the form

$$(4.5) \quad \Phi(\zeta) = \|\omega(\zeta, \zeta)\|_1 = \sum_{i=1}^{n_s} |\omega(\zeta_i, \zeta_i)| = \sum_{i=1}^{n_s} \omega(\zeta_i, \zeta_i); \quad \nabla_{\zeta} \Phi(\zeta) = \sum_{i=1}^{n_t} \frac{\partial \omega(\zeta_i, \zeta_i)}{\partial \zeta_i} \mathbf{e}_i.$$

4.1.7. Optimization algorithms. To solve the OED problem (2.8), we use Python's optimization routines provided in Scipy. Specifically, we use the implementation of L-BFGS-B [15, 42],

provided by `fmin_l_bfgs_b()` with a stopping criterion based on the maximum entry of the projected gradient. We set the tolerance to `pgtol` = 1×10^{-5} . This allows us to set bound constraints when needed, for example, when the SQRT kernel is invoked. The initial guess passed to the optimization algorithm is set to yield weighting values $\omega(\zeta_i, \zeta_i) = 0.5$; $i = 1, 2, \dots, n_s$. This means that all sensors are as likely to be activated as to be turned off.

4.2. Numerical results. We investigate several scenarios. The first case is where no observation correlations are considered; then we incorporate spatial correlations. The correlations are synthetically generated by using a Gaspari–Cohn function with a predefined length scale. Note that this choice is made for convenience to create synthetic covariances and is independent from the weighting function ρ used to control the temporal relative importance of observation covariances; see [Subsection 3.4](#). We use A-optimality as the main criterion for sensor placement in our numerical experiments. As discussed in [Section 3](#), we can use a randomized trace estimator to formulate the optimality criterion and the associated gradient. In our experiments we used the Hutchinson randomized trace estimator to approximate the A-optimality criterion, and we set the sample size to $n_r = 25$. This enabled us to carry out several comparative experiments both accurately and efficiently. Numerical results validating this assertion are given in [Appendix D.2](#). For fair comparison, we used the same realizations of random vectors to calculate the objective, namely, the optimality criterion, and the gradients in all experiments.

Note that while the A-optimality criterion is calculated based on the sum of the posterior variances discarding posterior covariances, it does in fact account for observation correlations, since posterior variances are influenced by both prior and observation error covariances (see [\(2.3\)](#)). Since the case with temporal observation correlations is not applicable here and since D-optimality might be more suitable for handling spatiotemporal observation correlations, we will leave the investigation of this case to future studies.

We are interested mainly in the design of an observational grid that will optimally serve the Bayesian retrieval of the goal QoI. Specifically, we are looking for the optimal subset of candidate sensor locations to deploy for data collection. We start by showing the results of solving the Bayesian inverse problem, with a fully deployed observational grid. [Figure 4](#) shows the ground truth, the prior, and the posterior prediction QoI γ obtained by solving the Bayesian inverse problem with all sensors activated. The results are shown for the case where no observation correlations are assumed, that is, when the correlation length scale is $\ell = 0$, and two experiments with space correlations with ℓ set to 1 and 3, respectively. This plot will serve as a visual benchmark as needed.

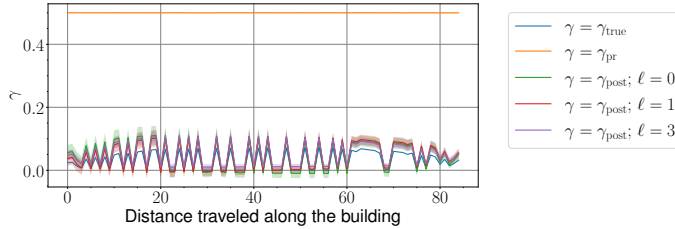


FIG. 4. The truth, the prior, and the posterior ($\pm 2\sigma_{\text{post}}$) prediction QoI γ . The truth is based on the ground truth of the model initial condition. The prior QoI is based on the mean of the prior distribution for all scenarios. The posterior prediction QoI is obtained by using the solution of the inverse problem, using all candidate sensors. The correlation length scale used in the Gaspari–Cohn function to construct correlations is indicated in the legends. The case when $\ell = 0$ corresponds to the diagonal covariance matrix, that is, no correlations, is assumed.

The goal of solving an OED problem is to find a small subset of sensors (e.g., given a limited budget) that yields a posterior QoI as close as possible to the ground truth shown in Figure 3(right), with minimum uncertainty. In what follows, we assume a maximum budget of λ observation sensors to be ideally placed in the domain. The solution of the OED problem is expected to be sparse but might not be binary. A simple rounding method to obtain a binary design is used when needed, by activating the sensors corresponding to the largest λ weights in the design resulting from solving an OED optimization problem. In our experiments, we show results for two choices of the budget λ : first, we set $\lambda = 8$, and second we set $\lambda = n_s/2$ where we allow up to 50% of the sensors to be activated. We discuss results obtained by solving the OED problem (2.8) with the A-optimality criterion $\Psi(\zeta) = \Psi^{GA}$, using the SQRT weighting kernel (3.7), the EXP kernel (3.8), and the logistic sigmoid kernels (3.9). Experiments are carried out for multiple values of the regularization parameter α , to study the effect of the regularization term on both sparsity and the order of relative importance of candidate sensors. We start with numerical experiments with uncorrelated observation errors, and then we show experiments with spatial observation correlations with multiple length scales, as described in Section 4.

4.2.1. No-correlations results. Figure 5 shows the optimal weights resulting from solving the OED problem with the SQRT weighting kernel and the logistic sigmoid kernel, respectively, for multiple values of the penalty parameter. Note that the EXP kernel and the sigmoid weighting functions lead to more sparse designs compared with the SQRT weighting kernel even with a penalty value $\alpha = 0$, that is, without enforcing a sparsity-promoting penalty term.

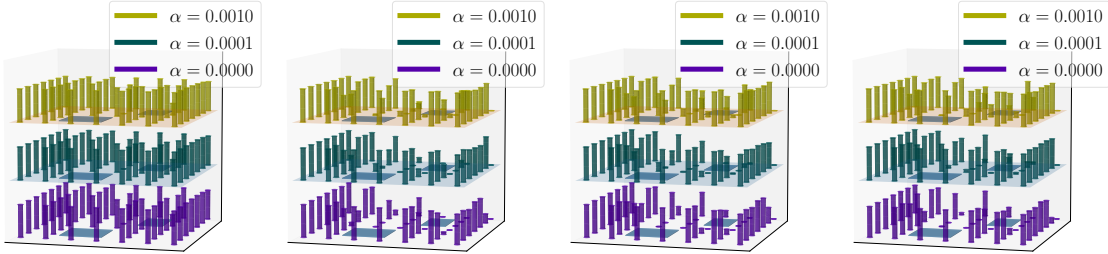


FIG. 5. Optimal weights resulting from solving the OED problem (2.8). Results are obtained (from left to right) by using the SQRT weighting kernel (3.7), the EXP kernel (3.8), and the logistic sigmoid kernels (3.9a), (3.9b) respectively, for values of the parameter α set to 0, $1e-4$, $1e-3$. The solution is plotted in the form of bars located on the grid, at the corresponding candidate sensor location. The height of each bar is set to the value of the weight obtained by solving (2.8). For a fair visual comparison, the weights are scaled to yield a maximum weight of 1, by dividing all weights by the maximum entry in the optimal solution. Thus we are actually plotting $\frac{\zeta^{\text{opt}}}{\|\zeta\|_{\infty}}$.

To better inspect the difference between the resulting optimal designs shown in Figure 5), we apply rounding to obtain a binary design, by activating the maximum $\lambda = 8$ sensors; the resulting binary designs are shown in Figure 6. The results in Figure 5 and Figure 6 indicate that, in general, increasing the value of the penalty parameter enforces sparsification on the solution of the OED problem. However, the optimal weights, the ranking, and the sparsity levels obtained by the four kernels are not identical. It would be hard, though, to judge which solution is better without inspecting two elements: the trace of the posterior covariance (i.e., the OED optimality criterion) and the quality of the solution of an inverse problem obtained by reconfiguring the observational grid based on the optimal weights obtained.

To be able to fairly judge the quality of the A-optimal designs, we inspect the value of the

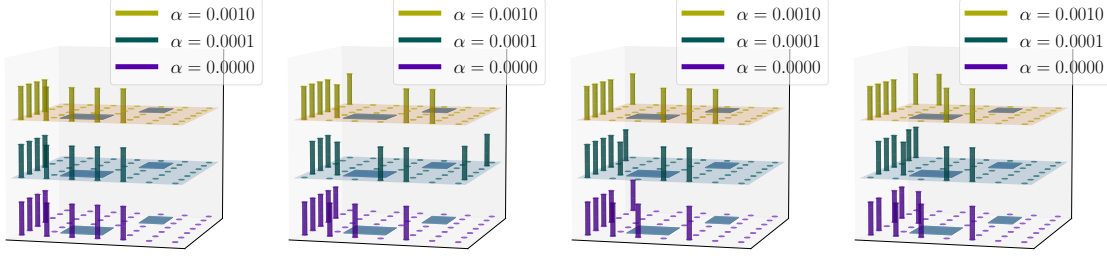


FIG. 6. Similar to Figure 5. Here, we show the binary design corresponding to the highest $\lambda = 8$ weights.

optimality criterion corresponding to the optimal solution. Table 1 shows the value of the A-optimality criterion, namely, the trace of the posterior covariance matrix, obtained by the optimal design before and after thresholding for multiple values of the penalty parameter α . Results are obtained by using the SQRT weighting kernel (3.7), the EXP kernel (3.8), and the logistic sigmoid kernels (3.9), respectively. For each choice of the weighting kernel, the first column shows the value of the posterior covariance trace obtained by setting the design to the solution of the relaxed OED problem (2.8), that is, $\Psi^{\text{GA}}(\zeta) = \text{Tr}(\Sigma_{\text{post}}(\zeta))$ with $\zeta = \zeta^{\text{opt}}$. The results in the second column correspond to the value of the optimality criterion $\Psi^{\text{GA}}(\zeta^{\text{b}})$, where ζ^{b} is a binary design obtained by setting the entries of ζ^{opt} corresponding to the highest $\lambda = 8$ weights to 1 and everything else to zero. The third column is similar to the second column, but the binary design is obtained by activating the sensors corresponding to the highest $n_s/2$ weights. The solutions obtained by using the EXP kernel and the sigmoid kernels exhibit lower values of the optimality criterion than those obtained by using the SQRT kernel.

TABLE 1

Value of the A-optimality criterion, namely, the trace of the posterior covariance matrix $\Psi^{\text{GA}}(\zeta) = \text{Tr}(\Sigma_{\text{post}}(\zeta))$, multiplied by 10^3 , obtained by the optimal design, before and after thresholding, for multiple values of the penalty parameter. Here, observations are assumed to be uncorrelated. Two thresholding/rounding approaches are used: (1) “Max 8,” in which the $\lambda = 8$ sensors with highest weights are activated, and (2) “Median,” in which all sensors with weights above the median value of the optimal weights are activated.

Regularization Penalty	SQRT Kernel (3.7)			EXP Kernel (3.8)			Sigmoid Kernel (3.9a)			Sigmoid Kernel (3.9b)		
	A-optimal Design	Thresholded Design Max 8	Median	A-optimal Design	Thresholded Design Max 8	Median	A-optimal Design	Thresholded Design Max 8	Median	A-optimal Design	Thresholded Design Max 8	Median
$\alpha = 0$	2.9790	323.5240	136.6920	0.1710	288.620	130.1060	0.1420	309.3490	111.60650	0.0020	181.6810	110.150
$\alpha = 1e-4$	2.9170	323.5240	136.6920	0.1040	155.2750	118.0930	0.1190	262.0170	137.56820	0.2070	259.2210	111.0860
$\alpha = 3e-4$	2.8110	323.5240	136.6920	0.1510	156.770	118.0930	0.1220	262.3410	127.61760	0.1430	131.8360	75.8280
$\alpha = 5e-4$	2.7160	323.5240	136.6920	0.0970	240.470	118.0930	0.070	265.5470	127.61760	0.1320	182.6640	114.0860
$\alpha = 1e-3$	2.5860	323.5240	136.6920	0.0850	235.1890	127.6180	0.1220	275.6280	118.09330	0.1710	266.9840	81.1980

Now, we turn our attention to the quality of the solution of an inverse problem (MAP point) obtained by reconfiguring the observational grid based on the optimal design. First, the observational grid is reconfigured as follows. We solve the A-OED problem to obtain the optimal design vector ζ^{opt} ; and then we calculate the vector of optimal weights $\omega(\zeta^{\text{opt}}, \zeta^{\text{opt}})$, which is then rounded to yield a binary design ζ^{b} . The resulting binary design ζ^{b} is used to reconfigure the observation grid, the observation operator—hence the forward operator \mathbf{F} — and the observation error covariance matrix. The inverse problem is then solved by using the reconfigured settings. Table 2 shows the RMSE results obtained by solving the inverse problem using the binary designs corresponding to optimal designs with objective values shown in Table 1. We also show the RMSE results corresponding to the prior QoI and the solution of the inverse problem with all sensors activated, setting a benchmark of the RMSE values. The four kernels yield optimal (rounded) designs that result in high-quality solutions of the inverse problems as suggested by the small RMSE values;

however, the EXP and the sigmoid kernels are generally better. Specifically, for a small budget of $\lambda = 8$ sensor, the RMSE results obtained by using the EXP and the sigmoid kernel are generally lower than that obtained by using the SQRT kernel. These results are also supported by the results in Figure 7, which display the solution of the inverse problem along with the associated posterior uncertainties. Thus, in the present setup, while the SQRT yields acceptable solution of the inverse problem (explained by the small values of the optimality criterion), both EXP and sigmoid functions yield higher weights to the more important sensors and achieve more accurate solutions of the inverse problem. Note that by allowing more sensors to be deployed, additional data is collected, and hence more information is gained. This is supported by the decrease in both objective values (Table 1) and the RMSE results (Table 2) when the number of sensors is increased from “Max 8” to “Median” rounding.

TABLE 2

Similar to Table 1. Here we show the RMSE results obtained by solving the inverse problem given the optimal design.

Regularization Penalty	RMSE									
	All Sensors		SQRT Kernel (3.7)		EXP Kernel (3.8)		Sigmoid Kernel (3.9a)		Sigmoid Kernel (3.9b)	
	Prior	Posterior	Max 8	Median	Max 8	Median	Max 8	Median	Max 8	Median
$\alpha = 0$	0.4704	0.0258	0.1710	0.0248	0.1812	0.0196	0.1429	0.0421	0.2029	0.1544
$\alpha = 1e-4$			0.1710	0.0248	0.0308	0.0340	0.1206	0.0320	0.1114	0.0428
$\alpha = 3e-4$			0.1710	0.0248	0.0455	0.0340	0.1098	0.0447	0.1310	0.0736
$\alpha = 5e-4$			0.1710	0.0248	0.0942	0.0340	0.1226	0.0447	0.0493	0.0221
$\alpha = 1e-3$			0.1710	0.0248	0.0922	0.0447	0.1146	0.0340	0.1133	0.0235

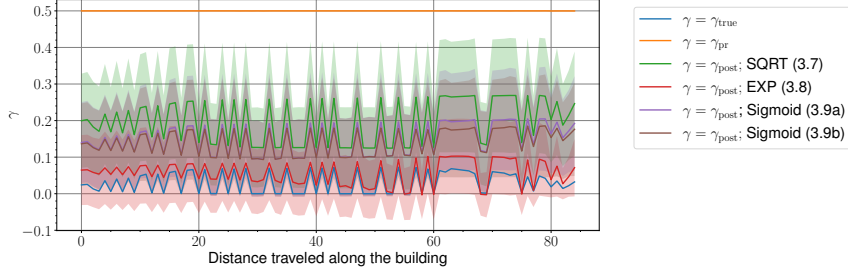
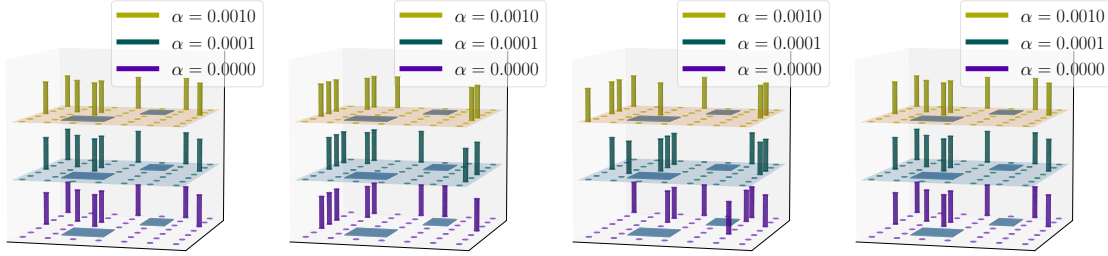
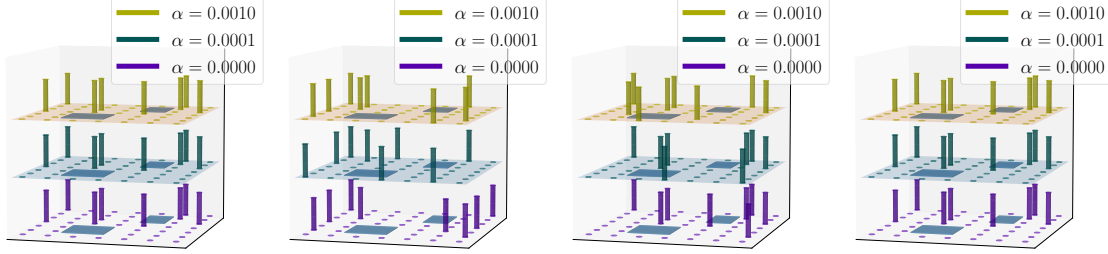


FIG. 7. Solution of the inverse problem, along with associated uncertainty ($\pm 2\sigma_{\text{post}}$), obtained based on the rounded A-optimal design resulting from solving the OED problem (2.8) with multiple choices of weighting kernel. Here, observations are assumed to be uncorrelated, and we show results obtained with $\alpha = 1e-4$ and with $\lambda = 8$ sensors activated. Inversion results here correspond to the second row of results in Table 2.

4.2.2. Space-correlations results. Here we show the results of experiments carried out with spatially correlated observations. Figure 8 shows the rounded binary designs obtained by setting the correlation length scale to $\ell = 1$, and Figure 9 shows binary designs for $\ell = 3$. Similar to the discussion in Subsection 4.2.1, results are shown here for multiple values of the penalty parameter α . These results (in comparison with Figure 6) indicate that discarding the observation correlations in an OED problem results in different optimal designs and thus can greatly degrade the quality of the solution of an inverse problem. Moreover, in the presence of spatial correlations between neighboring candidate sensor locations, the optimal design tends to be more spread in the domain.

To understand the empirical performance of the experiments carried out with observation spatial correlations, we analyze the value of the optimality criterion (Table 3) as well as the RMSE results (Table 4). Table 3 shows the value of the A-optimality criterion, namely, the trace of the

FIG. 8. Similar to Figure 6. Here we allow observation correlations with length scale $\ell = 1$.FIG. 9. Similar to Figure 6. Here we allow observation correlations with length scale $\ell = 3$.

posterior covariance matrix, obtained by the optimal design, before and after thresholding, for multiple values of the penalty parameter α . The overall performance explained by results in Table 3 is similar to the case where no observation correlations are involved, as explained by Table 1. Table 4 shows the RMSE of the solution of the inverse problem corresponding to optimal designs with objective values displayed in Table 3. We note that with a wider correlation length scale, that is, by allowing more sensors to be highly correlated, fewer sensors are required to achieve high accuracy. This is explained by the significant drop in RMSE values from $\ell = 1$ to $\ell = 3$. This is also obvious by comparing the RMSE results in Table 4 with Table 2.

TABLE 3

Similar to Table 1. Here we allow observation correlations, with correlation length scale ℓ set to $\ell = 1$ and $\ell = 3$, respectively.

Correlation Length-scale	Regularization Penalty	SQRT Kernel (3.7)			EXP Kernel (3.8)			Sigmoid Kernel (3.9a)			Sigmoid Kernel (3.9b)		
		A-optimal Design	Thresholded Design Max 8	Median	A-optimal Design	Thresholded Design Max 8	Median	A-optimal Design	Thresholded Design Max 8	Median	A-optimal Design	Thresholded Design Max 8	Median
$\ell = 1$	$\alpha = 0$	2.9270	66.2340	39.6990	0.1190	141.3830	61.4060	0.0010	43.350	22.6820	3.2770	66.2340	39.6990
	$\alpha = 1e-4$	2.5150	66.2340	39.6990	0.1360	114.7860	66.1020	0.0020	48.0670	23.0770	3.1540	66.2340	39.6990
	$\alpha = 3e-4$	2.8050	66.2340	39.6990	0.0940	119.9670	93.1980	0.1170	53.7270	41.6270	7.7680	66.2340	39.6990
	$\alpha = 5e-4$	2.720	66.2340	39.6990	0.0880	101.5260	87.590	0.0960	98.2240	80.5870	0.0010	130.0250	60.9430
	$\alpha = 1e-3$	9.1830	141.2610	60.6790	0.070	154.3130	73.650	0.1140	98.2240	83.5540	0.0010	8.2160	7.0340
$\ell = 3$	$\alpha = 0$	1.0370	9.5420	7.5420	0.1270	50.1230	21.80	0.0010	9.1830	7.5820	101.130	9.5420	7.590
	$\alpha = 1e-4$	1.2320	9.5420	7.5820	0.0990	99.6740	22.5040	0.0010	11.5650	7.7260	2.2540	9.5420	7.5820
	$\alpha = 3e-4$	1.2180	9.5420	7.5820	0.0920	63.8460	21.2640	0.0010	43.9660	15.4170	1.6890	9.5420	7.5820
	$\alpha = 5e-4$	4.5830	9.4380	7.6040	0.0920	59.2980	19.6270	0.0010	11.7370	7.6040	1.6760	9.5420	7.5820
	$\alpha = 1e-3$	17.3160	9.5420	7.5820	0.0710	51.3430	14.6530	0.160	9.1830	7.5820	1.6670	9.5420	7.5820

We conclude this section by showing the solution of the inverse problem obtained by reconfiguring the observational setup based on the A-optimal design resulting from (2.8) in the presence of observation correlations; see Figure 10. These results support our assertion that with increasing correlation length scale, fewer sensors are needed achieve high levels of accuracy.

The numerical results presented in this section reveal that solving an OED problem for sensor placement before carrying out Bayesian inversion is an essential step to guarantee an optimal deployment of observational grid under a limited budget. While the traditional formulation of the OED problem is useful, its performance can be enhanced by employing the generalized formulation

TABLE 4

Similar to Table 2. Here we allow observation correlations, with correlation length scale ℓ set to $\ell = 1$ and $\ell = 3$, respectively.

Correlation Length-scale	Regularization Penalty	RMSE									
		All Sensors		SQRT Kernel (3.7)		EXP Kernel (3.8)		Sigmoid Kernel (3.9a)		Sigmoid Kernel (3.9b)	
		Prior	Posterior	Max 8	Median	Max 8	Median	Max 8	Median	Max 8	Median
$\ell = 1$	$\alpha = 0$	0.4704	0.0225	0.1127	0.0942	0.0914	0.0550	0.0908	0.0800	0.1127	0.0942
	$\alpha = 1e-4$			0.1127	0.0942	0.0801	0.0840	0.0709	0.0777	0.1127	0.0942
	$\alpha = 3e-4$			0.1127	0.0942	0.0759	0.0331	0.0920	0.0932	0.1127	0.0942
	$\alpha = 5e-4$			0.1127	0.0942	0.0312	0.0328	0.0806	0.0621	0.1785	0.1238
	$\alpha = 1e-3$			0.1887	0.1503	0.0561	0.0453	0.0806	0.0390	0.0296	0.0248
$\ell = 3$	$\alpha = 0$	0.4704	0.0239	0.0292	0.0129	0.0825	0.0906	0.0360	0.0106	0.0292	0.0066
	$\alpha = 1e-4$			0.0290	0.0106	0.0991	0.1053	0.0386	0.0200	0.0292	0.0106
	$\alpha = 3e-4$			0.0290	0.0106	0.1139	0.0542	0.1341	0.0603	0.0290	0.0106
	$\alpha = 5e-4$			0.0436	0.0116	0.1213	0.1661	0.0609	0.0116	0.0292	0.0106
	$\alpha = 1e-3$			0.0290	0.0106	0.1304	0.0687	0.0360	0.0106	0.0292	0.0106

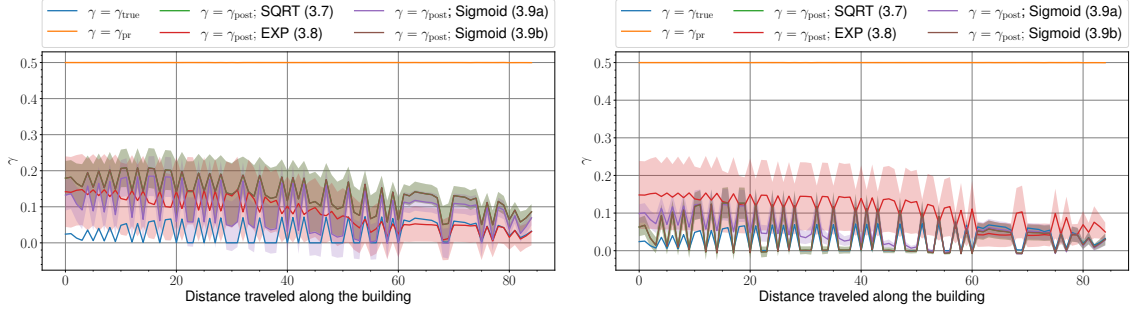


FIG. 10. Similar to Figure 7. Here observations are assumed to be correlated with length scale ℓ , with $\ell = 1$ (left), and $\ell = 3$ (right), respectively. We show results obtained with $\alpha = 1e-4$, and $\lambda = 8$ sensors are activated.

suggested in this work, especially in the presence of observation correlations. Specifically, while it can be tempting for simplicity, by ignoring observation correlations in the process of solving an OED problem, one will likely end up with a suboptimal design that can lead to erroneous solution of the inverse problem.

5. Conclusion. In this work, we presented a generalized approach for optimal experimental design for linear Bayesian inverse problems where the measurement errors are generally correlated. This study supplements the fast-evolving literature on OED for the Bayesian inverse problem; it provides an extended mathematical formulation of the most popular optimality criteria, as well as the associated gradients, essential for the numerical solution of the optimization problem. The proposed formulation follows a Hadamard product approach to formulate the weighted likelihood, which is then used in the optimality criterion. This approach provides a clear understanding of the effect of the design on the measurements and the covariances of observational errors and is valid in both finite- and infinite-dimensional settings of Bayesian linear inverse problems. We show that the traditional formulation of the OED problem is a special case of the proposed approach, where the observation precision matrix is weighted by a square root function. The Hadamard product formulation is shown to be more flexible, especially for handling spatiotemporal correlations. We provide multiple candidates of the weighting function that evaluates the relative importance of observation covariances. Our numerical results show that by choosing an exponential or a logistic sigmoid weighting kernel, we can achieve better results than by using the traditional formulation, that is, by using a square root weighting kernel. All weighting functions investigated here achieved similar performance in the presence of observation correlations with larger length scale, that is, by allowing more sensors to be correlated. However, by using a logistic sigmoid function for covariance weighting, the OED optimization problem transforms into an unconstrained optimization problem, which is generally easier to solve than the traditional OED problem with box constraints.

While we provided the mathematical formulation of the approach for A- and D-optimal designs, we focused our numerical experiments on A-optimality in the presence of spatial correlations. Extensions of the mathematical formulation and empirical studies of D-optimal designs in the presence of correlations in space and time domains are still required.

Appendix A. Weighing Kernels.

As explained in [Subsection 3.2](#), the weighting function $\omega(\zeta_i, \zeta_j)$ scales the (i, j) th entry of the precision matrix $\mathbf{\Gamma}_{\text{noise}}^{-1}$ and is utilized by the penalty function $\Phi(\zeta)$ in the regularization term of the optimization problem (2.8), to control the sparsity of the design.

Here, we discuss in detail multiple forms of the spatial weighting function ω and the associated derivatives, needed to construct the vectors of partial derivatives ([Equation \(3.11\)](#), [Equation \(3.22\)](#)). We use an idealized two-dimensional setup to visually explain the effect of the weighting functions. We start with a square root kernel (SQRT), then an exponential kernel (EXP), and finally a logistic-sigmoid (SIGMOID) kernel.

A.1. Square root (SQRT) weighting kernel. In this case the weighting kernel takes the following form:

$$(A.1) \quad \begin{aligned} \omega(\zeta_i, \zeta_j) &= \sqrt{\zeta_i} \sqrt{\zeta_j}, \\ \frac{\partial \omega(\zeta_i, \zeta_j)}{\partial \zeta_k} &= \frac{1}{2} \left(\frac{\sqrt{\zeta_j}}{\sqrt{\zeta_i}} \delta_{i,k} + \frac{\sqrt{\zeta_i}}{\sqrt{\zeta_j}} \delta_{j,k} \right); \quad \zeta_i, \zeta_j \in [0, 1]; \quad i, j, k = 1, 2, \dots, n_s, \end{aligned}$$

where $\delta_{i,k}$ is the standard Kronecker delta function. The weighting function (A.1) is utilized twice in the OED solution process. First, $\omega(\zeta_i, \zeta_i)$ scales the uncertainty level associated with the i th candidate sensor location, and $\omega(\zeta_i, \zeta_j)$ scales the covariance between any pairs of observation gridpoints. Second, the value of the penalty function is evaluated based on the values of $\omega(\zeta_i, \zeta_i), \forall i = 1, 2, \dots, n_s$. To visually inspect these effects contributed by the SQRT kernel (A.1) to the OED problem, consider a two-dimensional case where two candidate sensor locations are proposed. [Figure 11](#) shows surface plots of the SQRT weighting kernel (A.1) and the penalty function (3.6) with $p = 1$.

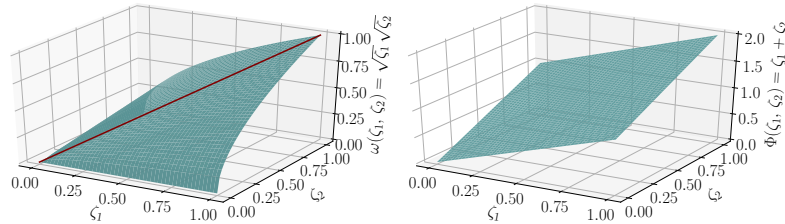


FIG. 11. Two-dimensional example showing the values of the SQRT weighting kernel (A.1), and the ℓ_1 -norm penalty function (3.6). Left: surface plot of the weighting function values. The red line shows the values used to damp the observation precisions, that is, the diagonal of $\mathbf{\Gamma}_{\text{noise}}$. Right: values of ℓ_1 penalty function with weight function (A.1).

The range of the weighting function is limited to the interval $[0, 1]$, only when the design space is restricted to the same interval. The value of the weighting function $\omega(\zeta_i, \zeta_j)$ is close to zero if any of the design variables ζ_i or ζ_j is close to zero regardless of the value of the other. This effect

is explained by the surface of the weighting function [Figure 11](#)(left) near the zero value of any of the design variables. This can potentially discard the information contributed by one sensor if it is correlated with another sensor associated with low weight.

A.2. Exponential (EXP) weighting kernel. The SQRT weighting function [\(A.1\)](#) requires solving a constrained optimization problem with domain constraints. To relax this requirement, one can use an exponential function where the design is allowed to assume any real value. In this case the weighting kernel and the associated derivative can take the form

$$(A.2) \quad \begin{aligned} \omega(\zeta_i, \zeta_j) &= e^{-a\zeta_i} e^{-a\zeta_j}, \\ \frac{\partial \omega(\zeta_i, \zeta_j)}{\partial \zeta_k} &= -a(\delta_{ik} + \delta_{jk}) \omega(\zeta_i, \zeta_j); \quad \zeta_i, \zeta_j \in \mathbb{R}; \quad i, j, k = 1, 2, \dots, n_s, \end{aligned}$$

where $a \geq 1$ is a scaling factor that controls the steepness of this kernel function. [Figure 12](#) shows the surface and the associated ℓ_1 norm of a two-dimensional design with the design weighting function defined by [\(A.2\)](#).

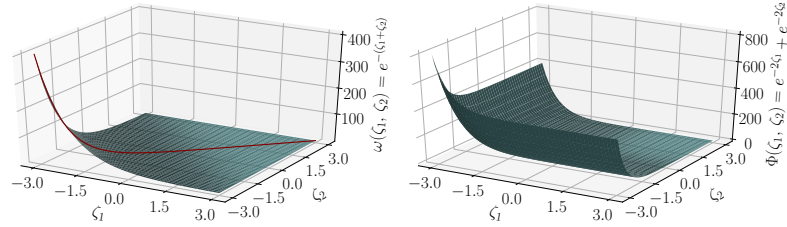


FIG. 12. Surface and ℓ_1 norm of an exponential weight function [\(A.2\)](#).

Unlike the SQRT kernel [\(A.1\)](#), the slope of this weighting function varies across the line $\zeta_i = \zeta_j$ (red line in [Figure 12](#)(left)). Specifically, in the case of an exponential kernel, the surfaces of both the weighting function [Figure 12](#)(left) and the penalty norm [Figure 12](#)(right) are steeper at lower values of the design variables, leading to smaller weights, which in turn promote sparsification. By allowing the design variables to take any real value, the value of the weight function can take any non-negative value. While this enables using any unconstrained optimization routine to solve the OED optimization problem, it makes the penalty term harder to adjust, because of the difference in scales. In order to restrict the range of the weighting kernel to the interval $[0, 1]$, the domain of the design variables must be set to $[0, \infty)$. Alternatively, to relax the requirement of any value-constraints on the design variables, one can use a sigmoid function (see [Appendix A.3](#)).

Note that an exponential kernel can take many other forms, such as $\omega(\zeta_i, \zeta_j) := e^{-a\zeta_i\zeta_j}$ or $\omega(\zeta_i, \zeta_j) := e^{-a\frac{\zeta_i+\zeta_j}{2}}$. This feature is discussed in the case of a logistic sigmoid kernel in the following section.

A.3. Logistic sigmoid (SIGMOID) weighting kernel. The logistic sigmoid function takes the form $f(x) = \frac{1}{1+e^{-ax}}$; $a \geq 1$, $x \in (-\infty, \infty)$, with a derivative satisfying the property $\frac{df}{dx} = af(x)f(1-x)$.

In this case the weighting kernel can take, for example, the form

$$(A.3a) \quad \omega(\zeta_i, \zeta_j) = \frac{1}{1+e^{-a\zeta_i}} \frac{1}{1+e^{-a\zeta_j}}; \quad a \geq 1, \zeta_i, \zeta_j \in (-\infty, \infty).$$

Figure 13 shows the surface and the associated ℓ_1 norm of a two-dimensional design with a standard logistic sigmoid kernel, that is, using weighting function defined by (A.3), with a scaling factor $a = 1$.

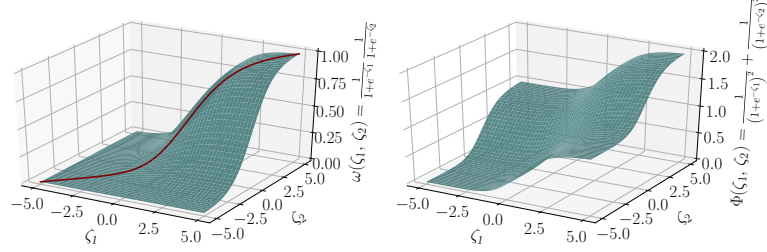


FIG. 13. Surface and ℓ_1 norm of sigmoid weight functions (A.3a).

The slope of the surface of the penalty term is close to zero near either bounds of the design domain, not only the lower bound. This not only can promote sparse weights but also can help obtain a near-binary solution. Similar to the SQRT kernel, however, the value of the weighting function is close to zero if any of the corresponding design variables is close to its lower bound regardless of the value of the other.

An alternative form of the sigmoid kernel is given by (A.3b). However, this form results in a saddle-point problem (see Figure 14):

$$(A.3b) \quad \omega(\zeta_i, \zeta_j) = \frac{1}{1 + e^{-a\zeta_i\zeta_j}}; \quad a \geq 1, \zeta_i, \zeta_j \in (-\infty, \infty).$$

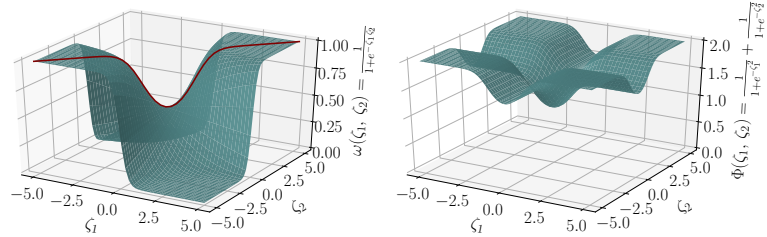


FIG. 14. Surface and ℓ_1 norm of sigmoid weight functions (A.3b).

In the numerical experiments carried out in this work (see Subsection 4.2), we utilize the logistic sigmoid weighting kernels defined on the form (A.3b), and (A.3c), with surface plots shown in Figure 14 and Figure 15, respectively. The form (A.3c) has a steeper surface near the values of the design close to the center of the domain and a slope close to zero near the bounds. Moreover, the slope of the penalty function (see Figure 15(right)) is close to zero near the bounds of the design domain. This is expected to promote binary design, while solving the OED optimization problem. Moreover, unlike the kernels defined by Equations (A.1, A.2, A.3a, A.3b), the value of the weight function affecting the correlations between candidate sensor locations is highly sensitive to each of the design variables associated with these sensor locations, even when one of the design

variable attains a value near its domain bounds.

$$(A.3c) \quad \omega(\zeta_i, \zeta_j) = \frac{1}{1 + \exp\left(-a \frac{\zeta_i + \zeta_j}{2}\right)}; \quad a \geq 1, \zeta_i, \zeta_j \in (-\infty, \infty).$$

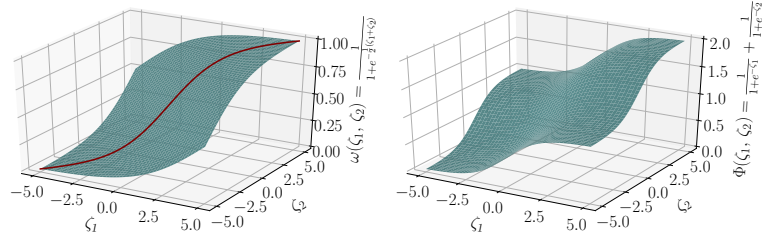


FIG. 15. Surface and ℓ_1 norm of sigmoid weight functions (A.3).

The coefficient a in (A.3c) can be set to a value greater than one, which increases the steepness of the weighting function surface; see, for example, Figure 16 for $a = 5$. This could be useful, for example, for applying a continuation procedure on the weighting kernel to escape local minima and possibly to induce a binary design. The continuation procedure can be carried out by re-solving the OED problem, using an increasing sequence of scaling factors. At each iteration of this procedure, the initial solution of the optimizer is set to the optimal solution resulting from using the previous scaling factor.

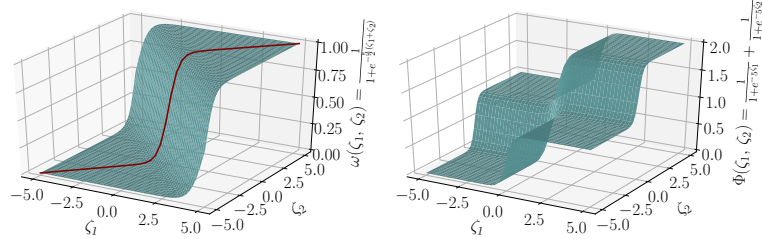


FIG. 16. Surface and ℓ_1 norm of sigmoid weight functions (A.3c).

Appendix B. A-Optimality Criterion and Gradient. Here, we detail the derivation of the formulae of the gradient of the A-optimality criterion (2.5) with respect to the design. Recall that for each $i = 1, 2, \dots, n_s$

$$(B.1) \quad \frac{\partial \Psi^{\text{GA}}(\zeta)}{\partial \zeta_i} = \text{Tr}\left(\frac{\partial \mathbf{P} \mathbf{\Gamma}_{\text{post}}(\zeta) \mathbf{P}^*}{\partial \zeta_i}\right) = -\text{Tr}\left(\mathbf{P} \mathbf{H}^{-1}(\zeta) \mathbf{F}^* \frac{\partial \mathbf{W}_{\Gamma}(\zeta)}{\partial \zeta_i} \mathbf{F} \mathbf{H}^{-1}(\zeta) \mathbf{P}^*\right).$$

B.1. Space correlations. In the case of temporally uncorrelated observations, by utilizing (3.12), then for each $i = 1, 2, \dots, n_s$

$$\begin{aligned} \frac{\partial \Psi^{\text{GA}}(\zeta)}{\partial \zeta_i} &= \text{Tr} \left(\mathbf{P} \mathbf{H}^{-1}(\zeta) \mathbf{F}^* \mathbf{W}_\Gamma(\zeta) \bigoplus_{m=1}^{n_t} \left(\mathbf{e}_i ((\mathbf{R}_m \mathbf{e}_i) \odot \eta_i)^\top + ((\mathbf{R}_m \mathbf{e}_i) \odot \eta_i) \mathbf{e}_i^\top \right) \mathbf{W}_\Gamma(\zeta) \mathbf{F} \mathbf{H}^{-1}(\zeta) \mathbf{P}^* \right) \\ &= 2 \text{Tr} \left(\mathbf{P} \mathbf{H}^{-1}(\zeta) \mathbf{F}^* \mathbf{W}_\Gamma(\zeta) \bigoplus_{m=1}^{n_t} ((\mathbf{R}_m \mathbf{e}_i) \odot \eta_i) \mathbf{e}_i^\top \mathbf{W}_\Gamma(\zeta) \mathbf{F} \mathbf{H}^{-1}(\zeta) \mathbf{P}^* \right), \end{aligned} \quad (\text{B.2})$$

where the vector of weight derivatives η_i is given by (3.11). Since observation errors are assumed to be temporally uncorrelated (i.e., across observation time instances t_m), then, given Equation (B.2), the gradient of the A-optimality criterion can be written in terms of cardinality vectors $\mathbf{e}_i \in \mathbb{R}^{n_s}$, as $\nabla_\zeta \Psi^{\text{GA}}(\zeta) = \sum_{i=1}^{n_s} \frac{\partial \Psi^{\text{GA}}(\zeta)}{\partial \zeta_i} \mathbf{e}_i$, resulting in the following form:

$$\begin{aligned} \nabla_\zeta \Psi^{\text{GA}}(\zeta) &= 2 \sum_{i=1}^{n_s} \mathbf{e}_i \text{Tr} \left(\mathbf{P} \mathbf{H}^{-1}(\zeta) \mathbf{F}^* \mathbf{W}_\Gamma(\zeta) \left(\bigoplus_{m=1}^{n_t} (((\mathbf{R}_m \mathbf{e}_i) \odot \eta_i) \mathbf{e}_i^\top) \right) \mathbf{W}_\Gamma(\zeta) \mathbf{F} \mathbf{H}^{-1}(\zeta) \mathbf{P}^* \right) \\ &= 2 \sum_{j=1}^{n_s} \mathbf{e}_i \text{Tr} \left(\mathbf{P} \mathbf{H}^{-1}(\zeta) \sum_{m=1}^{n_t} \mathbf{F}_{m,0}^* \mathbf{V}_m^\dagger(\zeta) ((\mathbf{R}_m \mathbf{e}_i) \odot \eta_i) \mathbf{e}_i^\top \mathbf{V}_m^\dagger(\zeta) \mathbf{F}_{0,m} \mathbf{H}^{-1}(\zeta) \mathbf{P}^* \right) \\ &= 2 \sum_{m=1}^{n_t} \sum_{j=1}^{n_s} \mathbf{e}_i \text{Tr} (\mathbf{e}_i^\top \mathbf{V}_m^\dagger(\zeta) \mathbf{F}_{0,m} \mathbf{H}^{-1}(\zeta) \mathbf{P}^* \mathbf{P} \mathbf{H}^{-1}(\zeta) \mathbf{F}_{m,0}^* \mathbf{V}_m^\dagger(\zeta) ((\mathbf{R}_m \mathbf{e}_i) \odot \eta_i) \mathbf{e}_i^\top) \\ &= 2 \sum_{j=1}^{n_s} \mathbf{e}_i \mathbf{e}_i^\top \sum_{m=1}^{n_t} \mathbf{V}_m^\dagger(\zeta) \mathbf{F}_{0,m} \mathbf{H}^{-1}(\zeta) \mathbf{P}^* \mathbf{P} \mathbf{H}^{-1}(\zeta) \mathbf{F}_{m,0}^* \mathbf{V}_m^\dagger(\zeta) ((\mathbf{R}_m \mathbf{e}_i) \odot \eta_i) \mathbf{e}_i^\top, \end{aligned} \quad (\text{B.3})$$

where as defined by (3.13),

$$\begin{aligned} \mathbf{W}_\Gamma(\zeta) &= \bigoplus_{m=1}^{n_t} (\mathbf{V}_m^\dagger(\zeta)), \quad \mathbf{L} = \bigoplus_{m=1}^{n_t} (\mathbf{L}_m), \\ \mathbf{V}_m^\dagger(\zeta) &:= \mathbf{L}_m^\top \mathbf{V}_m^{-1}(\zeta) \mathbf{L}_m, \quad \mathbf{V}_m(\zeta) := \mathbf{L}_m \left(\mathbf{R}_m \odot \left(\sum_{i,j=1}^{n_s} \omega(\zeta_i, \zeta_j) \mathbf{e}_i \mathbf{e}_j^\top \right) \right) \mathbf{L}_m^\top, \end{aligned} \quad (\text{B.4})$$

and we used the circular property of matrix trace and the fact that, for a symmetric matrix \mathbf{A} and a vector \mathbf{y} with conformable shapes, then $\mathbf{A} \odot (\mathbf{e}_i \mathbf{y}^\top) = \mathbf{e}_i ((\mathbf{e}_i^\top \mathbf{A}) \odot \mathbf{y}^\top) = \mathbf{e}_i ((\mathbf{A} \mathbf{e}_i) \odot \mathbf{y})^\top$. By utilizing the matrix of weights derivatives \mathbf{W}' defined by (3.15), we can refine (B.3) to

$$\nabla_\zeta \Psi^{\text{GA}}(\zeta) = 2 \sum_{m=1}^{n_t} \text{diag} (\mathbf{V}_m^\dagger(\zeta) \mathbf{F}_{0,m} \mathbf{H}^{-1}(\zeta) \mathbf{P}^* \mathbf{P} \mathbf{H}^{-1}(\zeta) \mathbf{F}_{m,0}^* \mathbf{V}_m^\dagger(\zeta) (\mathbf{R}_m \odot \mathbf{W}')) . \quad (\text{B.5})$$

B.2. Spatiotemporal correlations. In the presence of spatiotemporal correlations, the derivative of the A-optimality criterion is obtained as follows. For each $i = 1, 2, \dots, n_s$

$$\begin{aligned}
 \frac{\partial \Psi^{\text{GA}}(\zeta)}{\partial \zeta_i} &= -\text{Tr} \left(\mathbf{P} \mathbf{H}^{-1}(\zeta) \mathbf{F}^* \frac{\partial \mathbf{W}_\Gamma(\zeta)}{\partial \zeta_i} \mathbf{F} \mathbf{H}^{-1}(\zeta) \mathbf{P}^* \right) \\
 &= 2\text{Tr} \left(\mathbf{P} \mathbf{H}^{-1}(\zeta) \mathbf{F}^* \mathbf{W}_\Gamma(\zeta) \left(\sum_{m=1}^{n_t} ((\mathbf{\Gamma}_{\text{noise}} \mathbf{e}_q) \odot \vartheta_{i,m}) \mathbf{e}_q^\top \right) \mathbf{W}_\Gamma(\zeta) \mathbf{F} \mathbf{H}^{-1}(\zeta) \mathbf{P}^* \right) \\
 &= 2\text{Tr} \left(\mathbf{e}_q^\top \mathbf{W}_\Gamma(\zeta) \mathbf{F} \mathbf{H}^{-1}(\zeta) \mathbf{P}^* \mathbf{P} \mathbf{H}^{-1}(\zeta) \mathbf{F}^* \mathbf{W}_\Gamma(\zeta) \sum_{m=1}^{n_t} ((\mathbf{\Gamma}_{\text{noise}} \mathbf{e}_q) \odot \vartheta_{i,m}) \right) \\
 &= 2\mathbf{e}_q^\top \mathbf{W}_\Gamma(\zeta) \mathbf{F} \mathbf{H}^{-1}(\zeta) \mathbf{P}^* \mathbf{P} \mathbf{H}^{-1}(\zeta) \mathbf{F}^* \mathbf{W}_\Gamma(\zeta) \sum_{m=1}^{n_t} ((\mathbf{\Gamma}_{\text{noise}} \mathbf{e}_q) \odot \vartheta_{i,m}) ,
 \end{aligned}
 \tag{B.6}$$

where $q = i + (m-1)n_s$ and the vector of weights derivatives $\vartheta_{i,m}$ is defined by (3.22). The gradient of the A-optimality criterion can be written as

$$\begin{aligned}
 \nabla_\zeta \Psi^{\text{GA}}(\zeta) &= 2 \sum_{i=1}^{n_s} \mathbf{e}_i \mathbf{e}_{i+(n-1)n_s}^\top \mathbf{W}_\Gamma(\zeta) \mathbf{F} \mathbf{H}^{-1}(\zeta) \mathbf{P}^* \mathbf{P} \mathbf{H}^{-1}(\zeta) \mathbf{F}^* \mathbf{W}_\Gamma(\zeta) \sum_{m=1}^{n_t} ((\mathbf{\Gamma}_{\text{noise}} \mathbf{e}_q) \odot \vartheta_{i,m}) \\
 &= 2 \sum_{i=1}^{n_s} \sum_{m=1}^{n_t} \mathbf{e}_i \mathbf{e}_q^\top \mathbf{W}_\Gamma(\zeta) \mathbf{F} \mathbf{H}^{-1}(\zeta) \mathbf{P}^* \mathbf{P} \mathbf{H}^{-1}(\zeta) \mathbf{F}^* \mathbf{W}_\Gamma(\zeta) ((\mathbf{\Gamma}_{\text{noise}} \mathbf{e}_q) \odot \vartheta_{i,n}) .
 \end{aligned}
 \tag{B.7}$$

B.3. A-optimal design with randomized trace estimator. A randomized approximation of the A-optimality criterion $\tilde{\Psi}^{\text{GA}}(\zeta) \approx \Psi^{\text{GA}}(\zeta)$, as defined by (3.26), takes the form

$$\tilde{\Psi}^{\text{GA}}(\zeta) = \frac{1}{n_r} \sum_{r=1}^{n_r} \mathbf{z}_r^\top \Sigma_{\text{post}}(\zeta) \mathbf{z}_r = \frac{1}{n_r} \sum_{r=1}^{n_r} \mathbf{z}_r^\top \mathbf{P} \left(\mathbf{F} (\mathbf{\Gamma}_{\text{noise}} \odot \mathbf{W})^{-1} \mathbf{F}^* + \mathbf{\Gamma}_{\text{pr}}^{-1} \right)^{-1} \mathbf{P}^* \mathbf{z}_r ,
 \tag{B.8}$$

with $\mathbf{z}_r \in \mathbb{R}^{N_{\text{goal}}}$. The gradient of this criterion follows directly as

$$\frac{\partial \tilde{\Psi}^{\text{GA}}(\zeta)}{\partial \zeta_i} = \frac{1}{n_r} \sum_{r=1}^{n_r} \mathbf{z}_r^\top \mathbf{P} \mathbf{H}(\zeta)^{-1} \mathbf{F}^* \mathbf{W}_\Gamma(\zeta) \left(\mathbf{\Gamma}_{\text{noise}} \odot \frac{\partial \mathbf{W}}{\partial \zeta_i} \right) \mathbf{W}_\Gamma(\zeta) \mathbf{F} \mathbf{H}(\zeta)^{-1} \mathbf{P}^* \mathbf{z}_r .
 \tag{B.9}$$

This formula of the gradient can be refined given the exact formulation of the design matrix \mathbf{W} and its derivative $\frac{\partial \mathbf{W}_\Gamma}{\partial \zeta_i}$, as discussed before. If we assume the observation errors are temporally uncorrelated, then

$$\begin{aligned}
 \frac{\partial \tilde{\Psi}^{\text{GA}}(\zeta)}{\partial \zeta_i} &= \frac{1}{n_r} \sum_{r=1}^{n_r} \mathbf{z}_r^\top \mathbf{P} \mathbf{H}(\zeta)^{-1} \mathbf{F}^* \mathbf{W}_\Gamma(\zeta) \bigoplus_{m=1}^{n_t} \left(\mathbf{R}_m \odot \left(\mathbf{e}_i (\eta'_i)^\top + \eta'_i \mathbf{e}_i^\top \right) \right) \mathbf{W}_\Gamma(\zeta) \mathbf{F} \mathbf{H}(\zeta)^{-1} \mathbf{P}^* \mathbf{z}_r \\
 &= \frac{2}{n_r} \sum_{r=1}^{n_r} \sum_{m=1}^{n_t} (\xi_{r,m}^*)^\top \mathbf{e}_i ((\mathbf{R}_m \mathbf{e}_i) \odot \eta'_i)^\top \xi_{r,m} ,
 \end{aligned}
 \tag{B.10}$$

where the vectors $\xi_{r,m}$ and $\xi_{r,m}^*$ are given by

$$\xi_{r,m} = \mathbf{V}_m^\dagger(\zeta) \mathbf{F}_{0,m} \mathbf{H}(\zeta)^{-1} \mathbf{P}^* \mathbf{z}_r ; \quad (\xi_{r,m}^*)^\top = \mathbf{z}_r^\top \mathbf{P} \mathbf{H}(\zeta)^{-1} \mathbf{F}_{m,0}^* \mathbf{V}_m^\dagger(\zeta) ,
 \tag{B.11}$$

where $\mathbf{V}_m^\dagger(\zeta)$ is given by (B.4). The full gradient, written in terms of its components, in this case is

$$\begin{aligned} \nabla_\zeta \tilde{\Psi}^{\text{GA}}(\zeta) &= \frac{2}{n_r} \sum_{i=1}^{n_s} \mathbf{e}_i \sum_{r=1}^{n_r} \sum_{m=1}^{n_t} (\xi_{r,m}^*)^\top \mathbf{e}_i ((\mathbf{R}_m \mathbf{e}_i) \odot \eta_i')^\top \xi_{r,m} \\ &= \frac{2}{n_r} \sum_{r=1}^{n_r} \sum_{m=1}^{n_t} \xi_{r,m}^* \odot ((\mathbf{R}_m \odot \mathbf{W}') \xi_{r,m}) . \end{aligned} \quad (\text{B.12})$$

In the presence of spatiotemporal correlations, the gradient is found as follows:

$$\begin{aligned} \frac{\partial \tilde{\Psi}^{\text{GA}}(\zeta)}{\partial \zeta_i} &= \frac{1}{n_r} \sum_{r=1}^{n_r} \mathbf{z}_r^\top \mathbf{P} \mathbf{H}^{-1}(\zeta) \mathbf{F}^* \mathbf{W}_\Gamma(\zeta) \left(\Gamma_{\text{noise}} \odot \sum_{m=1}^{n_t} (\mathbf{e}_q \vartheta_{i,m}^\top + \vartheta_{i,m} \mathbf{e}_q^\top) \right) \mathbf{W}_\Gamma(\zeta) \mathbf{F} \mathbf{H}^{-1}(\zeta) \mathbf{P}^* \mathbf{z}_r \\ &= \frac{2}{n_r} \sum_{r=1}^{n_r} \mathbf{z}_r^\top \mathbf{P} \mathbf{H}^{-1}(\zeta) \mathbf{F}^* \mathbf{W}_\Gamma(\zeta) \left(\Gamma_{\text{noise}} \odot \sum_{m=1}^{n_t} (\mathbf{e}_q \vartheta_{i,m}^\top) \right) \mathbf{W}_\Gamma(\zeta) \mathbf{F} \mathbf{H}^{-1}(\zeta) \mathbf{P}^* \mathbf{z}_r \\ &= \frac{2}{n_r} \sum_{r=1}^{n_r} \sum_{m=1}^{n_t} \psi^* \mathbf{e}_q ((\Gamma_{\text{noise}} \mathbf{e}_q) \odot \vartheta_{i,m})^\top \psi_r , \end{aligned} \quad (\text{B.13})$$

where $q = i + (m-1)n_s$, $\psi_r = \mathbf{W}_\Gamma(\zeta) \mathbf{F} \mathbf{H}(\zeta)^{-1} \mathbf{P}^* \mathbf{z}_r$, and $\psi_r^* = \mathbf{z}_r^\top \mathbf{P} \mathbf{H}(\zeta)^{-1} \mathbf{F}^* \mathbf{W}_\Gamma(\zeta)$. The full gradient follows as

$$\begin{aligned} \nabla_\zeta \tilde{\Psi}^{\text{GA}}(\zeta) &= \frac{2}{n_r} \sum_{i=1}^{n_s} \mathbf{e}_i \sum_{r=1}^{n_r} \sum_{m=1}^{n_t} \psi_r^* \mathbf{e}_{i+(m-1)n_s} ((\Gamma_{\text{noise}} \mathbf{e}_{i+(m-1)n_s}) \odot \vartheta_{i,m})^\top \psi_r \\ &= \frac{2}{n_r} \sum_{r=1}^{n_r} \sum_{i=1}^{n_s} \sum_{m=1}^{n_t} \mathbf{e}_i \psi_r^* \mathbf{e}_{i+(m-1)n_s} ((\Gamma_{\text{noise}} \mathbf{e}_{i+(m-1)n_s}) \odot \vartheta_{i,m})^\top \psi_r . \end{aligned} \quad (\text{B.14})$$

Appendix C. D-Optimality Criterion and Gradient. When the D-optimality (2.5) is set as the OED criterion, that is, $\Psi^{\text{GD}}(\zeta) = \log \det(\Sigma_{\text{post}}(\zeta))$, the derivative w.r.t the design variables ζ_i , $i = 1, 2, \dots, n_s$, is

$$\begin{aligned} \frac{\partial \Psi^{\text{GD}}(\zeta)}{\partial \zeta_i} &= \text{Tr} \left(\Sigma_{\text{post}}^{-1}(\zeta) \frac{\partial \mathbf{P} \Gamma_{\text{post}}(\zeta) \mathbf{P}^*}{\partial \zeta_i} \right) \\ &= -\text{Tr} \left(\Sigma_{\text{post}}^{-1}(\zeta) \mathbf{P} \mathbf{H}^{-1}(\zeta) \mathbf{F}^* \frac{\partial \mathbf{W}_\Gamma}{\partial \zeta_i} \mathbf{F} \mathbf{H}^{-1}(\zeta) \mathbf{P}^* \right) . \end{aligned} \quad (\text{C.1})$$

C.1. Space correlations. For the sake of derivation, we define the Cholesky factorization of the prediction covariance as $\Sigma_{\text{post}}(\zeta) = \Sigma_{\text{post}}^{1/2} \Sigma_{\text{post}}^{T/2}$, with $\Sigma_{\text{post}}^{1/2}$ being the lower triangular factor. Moreover, the dimensionality of the prediction QoI is generally small, and such factorization if needed is inexpensive. Then, $\Sigma_{\text{post}}^{-1}(\zeta) = \Sigma_{\text{post}}^{-1/2} \Sigma_{\text{post}}^{-T/2}$ with $\Sigma_{\text{post}}^{-1/2} = (\Sigma_{\text{post}}^{1/2})^{-1}$. The gradient of

the D-optimality criterion follows as
(C.2)

$$\begin{aligned}
\nabla_{\zeta} \Psi^{\text{GD}}(\zeta) &= - \sum_{i=1}^{n_s} \mathbf{e}_i \text{Tr} \left(\Sigma_{\text{post}}^{-1}(\zeta) \mathbf{P} \mathbf{H}^{-1}(\zeta) \mathbf{F}^* \frac{\partial \mathbf{W}_{\Gamma}}{\partial \zeta_i} \mathbf{F} \mathbf{H}^{-1}(\zeta) \mathbf{P}^* \right) \\
&= \sum_{i=1}^{n_s} \mathbf{e}_i \text{Tr} \left(\Sigma_{\text{post}}^{-T/2} \mathbf{P} \mathbf{H}^{-1}(\zeta) \mathbf{F}^* \mathbf{W}_{\Gamma}(\zeta) \bigoplus_{m=1}^{n_t} \left(\mathbf{R}_m \odot \left(\mathbf{e}_i (\eta'_i)^{\top} + \eta'_i \mathbf{e}_i^{\top} \right) \right) \mathbf{W}_{\Gamma}(\zeta) \mathbf{F} \mathbf{H}^{-1}(\zeta) \mathbf{P}^* \Sigma_{\text{post}}^{-1/2} \right) \\
&= 2 \sum_{i=1}^{n_s} \mathbf{e}_i \text{Tr} \left(\Sigma_{\text{post}}^{-T/2} \mathbf{P} \mathbf{H}^{-1}(\zeta) \mathbf{F}^* \mathbf{W}_{\Gamma}(\zeta) \bigoplus_{m=1}^{n_t} \left(\mathbf{R}_m \odot \left(\eta'_i \mathbf{e}_i^{\top} \right) \right) \mathbf{W}_{\Gamma}(\zeta) \mathbf{F} \mathbf{H}^{-1}(\zeta) \mathbf{P}^* \Sigma_{\text{post}}^{-1/2} \right) \\
&= 2 \sum_{i=1}^{n_s} \mathbf{e}_i \sum_{m=1}^{n_t} \text{Tr} \left(\Sigma_{\text{post}}^{-T/2} \mathbf{P} \mathbf{H}^{-1}(\zeta) \mathbf{F}^* \mathbf{V}_{m,0}^{\dagger}(\zeta) \left((\mathbf{R}_m \mathbf{e}_i) \odot \eta'_i \right) \mathbf{e}_i^{\top} \mathbf{V}_m^{\dagger}(\zeta) \mathbf{F}_{0,m} \mathbf{H}^{-1}(\zeta) \mathbf{P}^* \Sigma_{\text{post}}^{-1/2} \right) \\
&= 2 \sum_{i=1}^{n_s} \mathbf{e}_i \mathbf{e}_i^{\top} \sum_{m=1}^{n_t} \mathbf{V}_m^{\dagger}(\zeta) \mathbf{F}_{0,m} \mathbf{H}^{-1}(\zeta) \mathbf{P}^* \Sigma_{\text{post}}^{-1}(\zeta) \mathbf{P} \mathbf{H}^{-1}(\zeta) \mathbf{F}^* \mathbf{V}_{m,0}^{\dagger}(\zeta) \left((\mathbf{R}_m \mathbf{e}_i) \odot \eta'_i \right) \\
&= 2 \sum_{m=1}^{n_t} \text{diag} \left(\mathbf{V}_m^{\dagger}(\zeta) \mathbf{F}_{0,m} \mathbf{H}^{-1}(\zeta) \mathbf{P}^* \Sigma_{\text{post}}^{-1}(\zeta) \mathbf{P} \mathbf{H}^{-1}(\zeta) \mathbf{F}^* \mathbf{V}_{m,0}^{\dagger}(\zeta) (\mathbf{R}_m \odot \mathbf{W}') \right),
\end{aligned}$$

where we used the circular property of matrix trace and the fact that the trace is invariant under matrix transposition, and $\mathbf{V}_m^{\dagger}(\zeta)$ is given by (B.4).

C.2. Spatiotemporal correlations. The gradient of the D-optimality criterion in this case is

$$\begin{aligned}
\nabla_{\zeta} \Psi^{\text{GD}}(\zeta) &= - \sum_{i=1}^{n_s} \mathbf{e}_i \text{Tr} \left(\Sigma_{\text{post}}^{-1} \mathbf{P} \mathbf{H}^{-1}(\zeta) \mathbf{F}^* \frac{\partial \mathbf{W}_{\Gamma}}{\partial \zeta_i} \mathbf{F} \mathbf{H}^{-1}(\zeta) \mathbf{P}^* \right) \\
&= \sum_{i=1}^{n_s} \mathbf{e}_i \text{Tr} \left(\Sigma_{\text{post}}^{-1} \mathbf{P} \mathbf{H}^{-1}(\zeta) \mathbf{F}^* \mathbf{W}_{\Gamma}(\zeta) \left(\mathbf{\Gamma}_{\text{noise}} \odot \sum_{m=1}^{n_t} \left(\mathbf{e}_q \vartheta_{i,m}^{\top} + \vartheta_{i,m} \mathbf{e}_q^{\top} \right) \right) \mathbf{W}_{\Gamma}(\zeta) \mathbf{F} \mathbf{H}^{-1}(\zeta) \mathbf{P}^* \right) \\
&= 2 \sum_{i=1}^{n_s} \mathbf{e}_i \text{Tr} \left(\Sigma_{\text{post}}^{-1} \mathbf{P} \mathbf{H}^{-1}(\zeta) \mathbf{F}^* \mathbf{W}_{\Gamma}(\zeta) \left(\mathbf{\Gamma}_{\text{noise}} \odot \sum_{m=1}^{n_t} \left(\mathbf{e}_q \vartheta_{i,m}^{\top} \right) \right) \mathbf{W}_{\Gamma}(\zeta) \mathbf{F} \mathbf{H}^{-1}(\zeta) \mathbf{P}^* \right) \\
&= 2 \sum_{i=1}^{n_s} \mathbf{e}_i \sum_{m=1}^{n_t} \text{Tr} \left(\Sigma_{\text{post}}^{-1} \mathbf{P} \mathbf{H}^{-1}(\zeta) \mathbf{F}^* \mathbf{W}_{\Gamma}(\zeta) \left(\mathbf{\Gamma}_{\text{noise}} \odot \left(\mathbf{e}_q \vartheta_{i,m}^{\top} \right) \right) \mathbf{W}_{\Gamma}(\zeta) \mathbf{F} \mathbf{H}^{-1}(\zeta) \mathbf{P}^* \right) \\
&= 2 \sum_{i=1}^{n_s} \mathbf{e}_i \sum_{m=1}^{n_t} \text{Tr} \left(\Sigma_{\text{post}}^{-1} \mathbf{P} \mathbf{H}^{-1}(\zeta) \mathbf{F}^* \mathbf{W}_{\Gamma}(\zeta) \mathbf{e}_q \left(\mathbf{\Gamma}_{\text{noise}} \mathbf{e}_q \odot \vartheta_{i,m} \right)^{\top} \mathbf{W}_{\Gamma}(\zeta) \mathbf{F} \mathbf{H}^{-1}(\zeta) \mathbf{P}^* \right) \\
&= 2 \sum_{i=1}^{n_s} \sum_{m=1}^{n_t} \mathbf{e}_i \left(\mathbf{\Gamma}_{\text{noise}} \mathbf{e}_q \odot \vartheta_{i,m} \right)^{\top} \mathbf{W}_{\Gamma}(\zeta) \mathbf{F} \mathbf{H}^{-1}(\zeta) \mathbf{P}^* \Sigma_{\text{post}}^{-1} \mathbf{P} \mathbf{H}^{-1}(\zeta) \mathbf{F}^* \mathbf{W}_{\Gamma}(\zeta) \mathbf{e}_q,
\end{aligned}$$

where $\mathbf{e}_q \equiv \mathbf{e}_{i+(m-1)n_s} \in \mathbb{R}^{N_{\text{obs}}}$; $i = 1, 2, \dots, n_s$, $m = 1, 2, \dots, n_t$.

Appendix D. Additional Numerical Results. In this section, we given additional empirical results to complement the work presented in [Section 4](#)

D.1. Reduced-order approximation of Hessian. Here, we give more details about the approach used to develop a reduced-order approximation of the Hessian operator in the Bayesian inverse problem. This complements the discussion in [Section 4](#)

Repeated evaluation of Hessian matrix-vector products is computationally demanding. We use the two-pass algorithm described in [\[41\]](#) to generate a randomized reduced-order approximation of the Hessian \mathbf{H} . The number of eigenvalues is set to 80, and the oversampling parameter is $p = 20$. [Figure 17](#) shows the leading $\lambda = 80$ eigenvalues, with approximation error. Fast decay

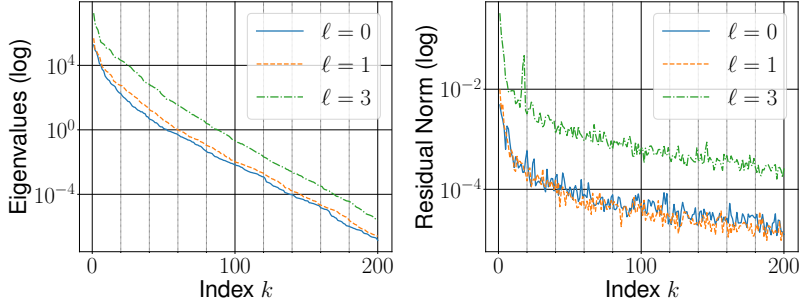


FIG. 17. Leading eigenvalues, on a logarithmic scale, of the Hessian \mathbf{H} obtained by the two-pass algorithm [\[41\]](#), along with the residual norms. Results are obtained with all sensors activated, i.e., $\zeta = \mathbf{1}$.

in eigenvalues, with over 99% of the variance explained by the leading 80 eigenvalues in all three cases, supports the accuracy of the reduced-order approximation of the Hessian.

D.2. Randomized estimator of the A-optimality criterion. In the numerical experiments [Section 4](#), we used the Hutchinson randomized trace estimator to approximate the A-optimality criterion, which enabled us to carry out several comparative experiments efficiently, and we set the sample size to $n_r = 25$, which achieved highly-accurate estimate of the optimality criterion.

To test the validity of this assertion, in our settings we compared the exact value of the posterior covariance trace with the randomized approximation. Results indicating the accuracy of the posterior trace approximation by randomization are shown in [Figure 18](#). The value of the Hutchinson randomized trace estimator was evaluated for the three experimental setups discussed in this section. In each case, the trace estimate of the posterior covariance matrix trace was evaluated by using several choices of the sample size n_r . For each experimental setting and for each choice of the sample size, the trace approximation was carried out 100 times, each with a new sample. The red stars show the true value of the posterior covariance trace in each case. These results show that even using a sample of size $n_r = 1$ generated, from Rademacher distribution, we obtain a good approximation of the trace of the posterior covariance matrix, albeit exhibiting high variability around the true value. A much better estimate of the true value can be obtained by increasing the sample size n_r . Thus, in our experiments, we followed this approach to approximate the A-optimality criterion, which enabled us to carry out several comparative experiments efficiently, and we set the sample size to $n_r = 25$.

Acknowledgments. This work was partially supported by the U.S. Department of Energy, Office of Science, Advanced Scientific Computing Research Program under contract DE-AC02-06CH11357 and Laboratory Directed Research and Development (LDRD) funding from Argonne

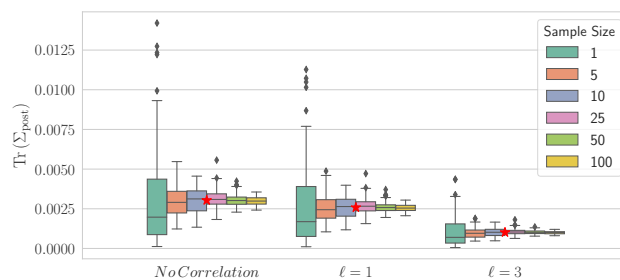


FIG. 18. Results showing accuracy of posterior trace approximation by randomization using the Hutchinson trace estimator. Box plots are shown for the three cases studied in this section. The first case considers the setup with no observation correlations, and the other cases correspond to the experiments where observation correlations are synthesized with length-scale ℓ set to 1 and 3, respectively. The true value of the posterior covariance trace $\text{Tr}(\Sigma_{\text{post}})$ is plotted as a red star for each case. In each case, the randomized trace is calculated by using various choices of the sample size n_r , where the random vectors are sampled from Rademacher distribution. The trace approximation is carried out 100 times for each choice of the sample size and for each case to generate the boxplots.

National Laboratory.

REFERENCES

- [1] A. ALEXANDERIAN, *Optimal experimental design for Bayesian inverse problems governed by PDEs: A review*, arXiv preprint arXiv:2005.12998, (2020).
- [2] A. ALEXANDERIAN, *Optimal experimental design for infinite-dimensional Bayesian inverse problems governed by PDEs: A review*, Inverse Problems, 37 (2021), p. 043001.
- [3] A. ALEXANDERIAN, P. J. GLOOR, O. GHATTAS, ET AL., *On Bayesian A-and D-optimal experimental designs in infinite dimensions*, Bayesian Analysis, 11 (2016), pp. 671–695.
- [4] A. ALEXANDERIAN, N. PETRA, G. STADLER, AND O. GHATTAS, *A-optimal design of experiments for infinite-dimensional Bayesian linear inverse problems with regularized ℓ_0 -sparsification*, SIAM Journal on Scientific Computing, 36 (2014), pp. A2122–A2148, <https://doi.org/10.1137/130933381>.
- [5] A. ALEXANDERIAN, N. PETRA, G. STADLER, AND O. GHATTAS, *A fast and scalable method for A-optimal design of experiments for infinite-dimensional Bayesian nonlinear inverse problems*, SIAM Journal on Scientific Computing, 38 (2016), pp. A243–A272, <https://doi.org/10.1137/140992564>.
- [6] A. ALEXANDERIAN AND A. K. SAIBABA, *Efficient D-optimal design of experiments for infinite-dimensional Bayesian linear inverse problems*, Submitted, (2017), <https://arxiv.org/abs/1711.05878>.
- [7] A. ATTIA, A. ALEXANDERIAN, AND A. K. SAIBABA, *Goal-oriented optimal design of experiments for large-scale Bayesian linear inverse problems*, Inverse Problems, 34 (2018), p. 095009.
- [8] A. ATTIA AND E. CONSTANTINESCU, *An optimal experimental design framework for adaptive inflation and covariance localization for ensemble filters*, arXiv preprint arXiv:1806.10655, (2018).
- [9] A. ATTIA AND A. SANDU, *A Hybrid Monte Carlo sampling filter for non-Gaussian data assimilation*, AIMS Geosciences, 1 (2015), pp. 4–1–78, <https://doi.org/http://dx.doi.org/10.3934/geosci.2015.1.41>.
- [10] A. ATTIA, R. ȘTEFĂNESCU, AND A. SANDU, *The reduced-order Hybrid Monte Carlo sampling smoother*, International Journal for Numerical Methods in Fluids, (2016), <https://doi.org/10.1002/fld.4255>.
- [11] H. AVRON AND S. TOLEDO, *Randomized algorithms for estimating the trace of an implicit symmetric positive semi-definite matrix*, Journal of the ACM (JACM), 58 (2011), pp. 1–34.
- [12] R. BANNISTER, *A review of operational methods of variational and ensemble-variational data assimilation*, Quarterly Journal of the Royal Meteorological Society, 143 (2017), pp. 607–633.
- [13] T. BUI-THANH, O. GHATTAS, J. MARTIN, AND G. STADLER, *A computational framework for infinite-dimensional Bayesian inverse problems part i: The linearized case, with application to global seismic inversion*, SIAM Journal on Scientific Computing, 35 (2013), pp. A2494–A2523.
- [14] T. BUI-THANH, O. GHATTAS, J. MARTIN, AND G. STADLER, *A computational framework for infinite-dimensional Bayesian inverse problems Part I: The linearized case, with application to global seismic inversion*, SIAM Journal on Scientific Computing, 35 (2013), pp. A2494–A2523, <https://doi.org/10.1137/12089586X>.
- [15] R. H. BYRD, P. LU, J. NOCEDAL, AND C. ZHU, *A limited memory algorithm for bound constrained optimization*, SIAM Journal on Scientific Computing, 16 (1995), pp. 1190–1208.

- [16] K. CHALONER AND I. VERDINELLI, *Bayesian experimental design: A review*, Statistical Science, 10 (1995), pp. 273–304.
- [17] N. CRESSIE AND C. K. WIKLE, *Statistics for spatio-temporal data*, John Wiley & Sons, 2015.
- [18] R. DALEY, *Atmospheric data analysis*, Cambridge University Press, 1991.
- [19] H. DETTE, A. PEPELYSHEV, A. ZHIGLJAVSKY, ET AL., *Optimal design for linear models with correlated observations*, The Annals of Statistics, 41 (2013), pp. 143–176.
- [20] V. FEDOROV AND J. LEE, *Design of experiments in statistics*, in Handbook of semidefinite programming, R. S. H. Wolkowicz and L. Vandenberghe, eds., vol. 27 of Internat. Ser. Oper. Res. Management Sci., Kluwer Acad. Publ., Boston, MA, 2000, pp. 511–532.
- [21] G. GASPARI AND S. E. COHN, *Construction of correlation functions in two and three dimensions*, Quarterly Journal of the Royal Meteorological Society, 125 (1999), pp. 723–757.
- [22] E. HABER, L. HORESH, AND L. TENORIO, *Numerical methods for experimental design of large-scale linear ill-posed inverse problems*, Inverse Problems, 24 (2008), pp. 125–137.
- [23] E. HABER, L. HORESH, AND L. TENORIO, *Numerical methods for the design of large-scale nonlinear discrete ill-posed inverse problems*, Inverse Problems, 26 (2010), p. 025002.
- [24] E. HABER, Z. MAGNANT, C. LUCERO, AND L. TENORIO, *Numerical methods for A-optimal designs with a sparsity constraint for ill-posed inverse problems*, Computational Optimization and Applications, (2012), pp. 1–22.
- [25] T. M. HAMILL AND J. S. WHITAKER, *Distance-dependent filtering of background error covariance estimates in an ensemble Kalman filter*, Monthly Weather Review, 129 (2001), pp. 2776–2790.
- [26] E. HERMAN, A. ALEXANDERIAN, AND A. K. SAIBABA, *Randomization and reweighted ℓ_1 -minimization for A-optimal design of linear inverse problems*, arXiv preprint arXiv:1906.03791, (2019).
- [27] R. A. HORN, *The Hadamard product*, vol. 40, American Mathematical Society, Proceedings of Symposia in Applied Mathematics, 1990, pp. 87–169.
- [28] X. HUAN AND Y. M. MARZOUK, *Simulation-based optimal Bayesian experimental design for nonlinear systems*, Journal of Computational Physics, 232 (2013), pp. 288–317, <https://doi.org/http://dx.doi.org/10.1016/j.jcp.2012.08.013>.
- [29] K. KOVAL, A. ALEXANDERIAN, AND G. STADLER, *Optimal experimental design under irreducible uncertainty for linear inverse problems governed by pdes*, Inverse Problems, (2020).
- [30] S. LIU, S. P. CHEPURI, M. FARDAD, E. MAŞAZADE, G. LEUS, AND P. K. VARSHNEY, *Sensor selection for estimation with correlated measurement noise*, IEEE Transactions on Signal Processing, 64 (2016), pp. 3509–3522.
- [31] A. MOOSAVI, A. ATTIA, AND A. SANDU, *Tuning covariance localization using machine learning*, in International Conference on Computational Science, Springer, 2019, pp. 199–212.
- [32] W. G. MÜLLER, *Collecting spatial data: Optimum design of experiments for random fields*, Springer Science & Business Media, 2007.
- [33] W. NÄTHER, *Effective observation of random fields*, vol. 72, Teubner, 1985.
- [34] I. M. NAVON, *Data assimilation for numerical weather prediction: a review*, in Data assimilation for atmospheric, oceanic and hydrologic applications, Springer, 2009, pp. 21–65.
- [35] A. PÁZMAN, *Foundations of optimum experimental design*, D. Reidel Publishing Co., 1986.
- [36] N. PETRA AND G. STADLER, *Model variational inverse problems governed by partial differential equations*, Tech. Report 11-05, The Institute for Computational Engineering and Sciences, The University of Texas at Austin, 2011.
- [37] J. PILZ AND J. PILZ, *Bayesian estimation and experimental design in linear regression models*, vol. 212, Wiley New York, 1991.
- [38] F. PUKELSHEIM, *Optimal design of experiments*, John Wiley & Sons, New-York, 1993.
- [39] S. SAGER, *Sampling decisions in optimum experimental design in the light of Pontryagin’s maximum principle*, SIAM Journal on Control and Optimization, 51 (2013), pp. 3181–3207.
- [40] A. K. SAIBABA, J. LEE, AND P. K. KITANIDIS, *Randomized algorithms for generalized hermitian eigenvalue problems with application to computing karhunen–loève expansion*, Numerical Linear Algebra with Applications, 23 (2016), pp. 314–339.
- [41] A. K. SAIBABA, J. LEE, AND P. K. KITANIDIS, *Randomized algorithms for generalized hermitian eigenvalue problems with application to computing karhunen–loève expansion*, Numerical Linear Algebra with Applications, 23 (2016), pp. 314–339.
- [42] SCIPY, *Python implementation of the L-BFGS-B algorithm*. https://docs.scipy.org/doc/scipy-0.14.0/reference/generated/scipy.optimize.fmin_l_bfgs_b.html, 2017.
- [43] D. UCIŃSKI, *Optimal sensor location for parameter estimation of distributed processes*, International Journal of Control, 73 (2000), pp. 1235–1248.
- [44] D. UCIŃSKI, *D-optimal sensor selection in the presence of correlated measurement noise*, Measurement, 164

- (2020), p. 107873.
- [45] D. UCIŃSKI AND A. C. ATKINSON, *Experimental design for time-dependent models with correlated observations*, Studies in Nonlinear Dynamics & Econometrics, 8 (2004).
 - [46] U. VILLA, N. PETRA, AND O. GHATTAS, *hIPPYlib: An extensible software framework for large-scale deterministic and linearized Bayesian inversion*, (2016). <http://hippylib.github.io>.
 - [47] J. S. WHITAKER AND T. M. HAMILL, *Ensemble data assimilation without perturbed observations*, Monthly Weather Review, 130 (2002), pp. 1913–1924.
 - [48] J. YU, V. M. ZAVALA, AND M. ANITESCU, *A scalable design of experiments framework for optimal sensor placement*, Journal of Process Control, (2017).